Journal of Colloid and Interface Science 449 (2015) 46–61

Contents lists available at ScienceDirect

Journal of Colloid and Interface Science

www.elsevier.com/locate/jcis

Solubility limits and phase diagrams for fatty alcohols in anionic (SLES) and zwitterionic (CAPB) micellar surfactant solutions

Sylvia S. Tzocheva [a], Krassimir D. Danov [a], Peter A. Kralchevsky [a,*], Gergana S. Georgieva [a], Albert J. Post [b], Kavssery P. Ananthapadmanabhan [b]

[a] Department of Chemical Engineering, Faculty of Chemistry & Pharmacy, Sofia University, 1164 Sofia, Bulgaria
[b] Unilever Research and Development, Trumbull, CT 06611, USA

ARTICLE INFO

Article history:
Received 14 August 2014
Accepted 17 September 2014
Available online 28 September 2014

This article is dedicated to Professor Darsh T. Wasan on the occasion of his 75th birthday.

Keywords:
Solubility limit of fatty alcohols
Fatty alcohols in surfactant micelles
Solubilization energy
Micellization of ionic surfactants
CMC for mixed micelles

ABSTRACT

By analysis of experimental data, a quantitative theoretical interpretation of the solubility limit of medium- and long-chain fatty alcohols in micellar solutions of water-soluble surfactants is presented. A general picture of the phase behavior of the investigated systems is given in the form of phase diagrams. The limited solubility of the fatty alcohols in the micelles of conventional surfactants is explained with the precipitation of their monomers in the bulk, rather than with micelle phase separation. The long chain fatty alcohols (with $n = 14$, 16 and 18 carbon atoms) exhibit an ideal mixing in the micelles of the anionic surfactant sodium laurylethersulfate (SLES) and the zwitterionic surfactant cocamidopropyl betaine (CAPB) at temperatures of 25, 30, 35 and 40 °C. Deviations from ideality are observed for the alcohols of shorter chain ($n = 10$ and 12), which can be explained by a mismatch with the longer chains of the surfactant molecules. Using the determined thermodynamic parameters of the systems, their phase diagrams are constructed. Such a diagram consists of four domains, viz. mixed micelles; coexistent micelles and precipitate (dispersed crystallites or droplets); precipitate without micelles, and molecular solution. The four boundary lines intersect in a quadruple point, Q. For ionic surfactants (like SLES), a detailed theory for calculating the boundary lines of the phase diagrams is developed and verified against data for the positions of the kinks in surface tension isotherms. The theory takes into account the electrostatic interactions in the micellar solutions and the effect of counterion binding. The results can be useful for a quantitative interpretation and prediction of the phase behavior of mixed solutions of two (or more) surfactants, one of them being water soluble and forming micelles, whereas the other one has a limited water solubility, but readily forms mixed micelles with the former surfactant.

1. Introduction

The fatty alcohols (alkanols) with $n \geqslant 10$ carbon atoms exhibit a low molecular solubility in water. However, they can be dissolved (solubilized) in surfactant micellar solutions, where they form mixed micelles with the basic surfactant. The micelles serve as carriers of fatty alcohol molecules during the processes of adsorption and formation of disperse systems (foams, emulsions and suspensions). The adsorption of fatty alcohols essentially influences the interfacial properties, as well as the dispersion stability and rheology.

For example, the incorporation of fatty acid or alcohol molecules in a surfactant adsorption layer is known to increase the surface elasticity and to render the mixed adsorption monolayers tangentially immobile. For example, in his study on the drainage of vertical foam films, Mysels et al. [1] distinguished two regimes: *mobile* films where the film thickness does not remain uniform and surface vortices are observed, and *rigid* films, which drain much more regularly. Typical examples for mobile films are those formed from pure sodium dodecylsulfate (SDS) solutions, and for rigid films – those formed from mixed SDS + dodecanol solutions [2]. The presence of fatty alcohol (or fatty acid) in the solution leads to a slower drainage of the produced foams. As demonstrated by Wasan et al. [3–5] and by other authors [6–8], the increased surface elasticity due to surface phase transitions leads to the formation of foams of much smaller bubbles and enhanced bulk viscoelasticity, which is important for the properties of many consumer products. Such effects have been observed with additives as dodecanol [9–13], lauric and myristic acids [13–16], as well as with sodium and potassium salts of the fatty acids [8,14,17].

* Corresponding author. Fax: +359 2 962 5643.
E-mail address: pk@lcpe.uni-sofia.bg (P.A. Kralchevsky).

http://dx.doi.org/10.1016/j.jcis.2014.09.042
0021-9797/

The fatty alcohols exhibit a limited solubility also in *micellar* surfactant solutions. Precipitate of fatty alcohol crystallites or droplets appears above a certain alcohol concentration, which is termed *solubility limit* or *saturation concentration*. The behavior of the non-dissociated (protonated) fatty acids is similar. In a recent study [18], we investigated the solubility limits of fatty acids in micellar solutions of the anionic surfactant sodium laurylethersulfate (SLES) and the zwitterionic surfactant cocamidopropyl betaine (CAPB). The saturation concentration was explained with the precipitation of fatty-acid crystallites when the concentration of monomers (that exist in equilibrium with the mixed micelles) reaches the solubility limit of the respective acid in pure water. By data analysis, the solubilization energy and interaction parameter for the fatty acid molecules in surfactant micelles were determined. Using these parameter values, phase diagrams of the investigated mixed solutions were constructed. The results enable one to interpret and predict the solubility and phase behavior of medium- and long-chain fatty acids in micellar surfactant solutions, as well as to determine the critical micellization concentration (CMC) for the respective mixed solutions [18].

The present study is aimed at extending our previous analysis for fatty acids to the case of fatty alcohols. In addition, the thermodynamic theory of the phase diagrams from Ref. [18], which is accurate for nonionic and zwitterionic surfactants, is extended to *ionic* surfactants by taking into account the electrostatic interactions in the micellar solutions and the effect of counterion binding [19,20]. Sections 3–5 of the present paper have a structure that is similar to the respective material in Ref. [18], which facilitates the comparison of the phase behavior of fatty acids and alcohols in micellar solutions. Section 6 presents the new detailed theory for the phase diagrams of fatty alcohols in ionic surfactant solutions.

In particular, Section 3 presents data for the solubility limits of saturated straight-chain fatty alcohols with $n = 10$, 12, 14, 16 and 18 carbon atoms in micellar SLES and CAPB solutions determined by turbidimetry at four different temperatures. The linear dependence between the solubility limit and the surfactant concentration, which has been established in Ref. [18] for fatty acids, is verified for fatty alcohols. In Section 4, the thermodynamic theory is applied to interpret the data and to determine the solubilization energy and the interaction parameter of the fatty alcohols in the mixed micelles with SLES and CAPB. The values of these parameters for fatty acids and alcohols are compared and discussed. In Section 5, using the determined parameter values, we construct phase diagrams for fatty alcohols in micellar solutions of the zwitterionic surfactant CAPB. In Section 6, the theory is extended to the case of ionic surfactants, and phase diagrams for fatty alcohols in micellar solutions of SLES are constructed. The diagrams are tested against experimental data for the surface tension of mixed solutions with SLES. It is explained why in some cases the *nonionic* approximation from Ref. [18] works very well for micellar solutions of *ionic* surfactants, but in other cases significant differences between the detailed and approximated theory are observed.

2. Materials and methods

The following straight-chain saturated fatty alcohols were used: 1-decanol (capric or decyl alcohol), 99%, from Sigma Aldrich; 1-dodecanol (lauryl alcohol), 98% from Sigma Aldrich; 1-tetradecanol (myristyl or tetradecyl alcohol), >98%, from Merck; 1-hexadecanol (cetyl or palmityl alcohol), 99%, from Sigma Aldrich, and 1-octadecanol (stearyl or octadecyl alcohol), >95%, from Fluka. For brevity, in the text these fatty alcohols are denoted by C_nOH at $n = 10$–18. All chemicals were used as received, without additional purification.

The anionic surfactant was sodium laurylethersulfate (SLES) with one ethylene-oxide group, product of Stepan Co.; commercial name STEOL CS-170; molecular mass 332.4 g/mol. The critical micellization concentration of STEOL CS-170 is $CMC_S = 0.7$ mM determined by both surface tension and conductivity measurements at 25 °C [18]; see also Refs. [21,22]. STEOL CS-170 contains alkyl chains in the range C10–16 (in average C12), which is the reason for its lower CMC. Note that the CMC of the pure sodium laurylethersulfate is 3 mM [23].

The zwitterionic surfactant with a quaternary ammonium cation was cocamidopropyl betaine (CAPB), product of Goldschmidt GmbH; commercial name Tego® Betain F50; molecular mass 356 g/mol. CAPB finds a wide application in personal-care detergency. The critical micellization concentration of CAPB is $CMC_S = 9 \times 10^{-5}$ M determined by surface tension measurements at 25 °C.

The solutions were prepared with deionized water (Milli-Q purification system, Millipore, USA) of specific resistivity 18.2 MΩ cm. The working procedure was as follows. First, the fatty alcohol was added to the micellar surfactant solution. Then, the solution was heated at 65 °C and stirred for 15 min. Next, it was placed in a thermostat, where it was kept for at least 24 h to equilibrate at the working temperature: 25, 30, 35 or 40 °C. The experiments were carried out at the natural pH of the prepared solutions, which is about 6.

The absorbance of light by the solutions was measured by a Unicam UV/VIS spectrophotometer (Unicam Ltd., Cambridge, UK) at wavelength $\lambda = 500$ nm. By definition, the absorbance is $A_\lambda = -\log_{10}(I_0/I)$, where I_0 and I are the intensities of the incident and transmitted beams. The turbidity is due to light scattering by fatty-alcohol precipitate, which consists of dispersed crystallites or droplets depending on the temperature and alcohol chainlength. The aim of these measurements was to determine the solubility limit of the fatty alcohols in the micelles, which is detected as an abrupt increase of the solution's turbidity due to the appearance of precipitate. The melting temperatures of the investigated fatty alcohols are 6.9; 23.9; 38.2; 49.2 and 57.9 °C for C_nOH at $n = 10$, 12, 14, 16 and 18, respectively [24]. Before each absorbance measurement, the flask with the solution was shaken to disperse the precipitate, if any. From the obtained data, we determined the solubilization constant of each fatty alcohol in the surfactant micelles at the respective temperature, as explained in Section 4.4.

3. Experimental results

3.1. Data for the solubility limit

Typical experimental curves for the light absorbance vs. the concentration of fatty alcohol in micellar solutions are shown in Fig. 1a for SLES and in Fig. 1b for CAPB (100 mM surfactant at 25 °C). In each separate curve, an abrupt increase in the absorbance is observed above a certain saturation concentration, which is denoted by $C_{A,sat}$ and indicates the appearance of fatty-alcohol precipitate in the solution.

The general tendency is $C_{A,sat}$ to decrease with the increase of the number of carbon atoms, n, in the fatty alcohol molecule C_nOH (Fig. 1). In other words, the solubility of C_nOH in the micelles of SLES and CAPB decreases with the increase of the fatty-alcohol chainlength. For $n = 14$, 16 and 18, the solubility limits are closer, whereas for $n = 10$ and 12 they are markedly higher.

The experimental values of $C_{A,sat}$ at 100 mM surfactant solutions are given in Table 1 for SLES and CAPB. The molar fraction of the fatty alcohol in the mixed micelles is calculated from the expression:

$$y_{A,sat} = \frac{C_{A,sat}}{C_S + C_{A,sat}} \tag{3.1}$$

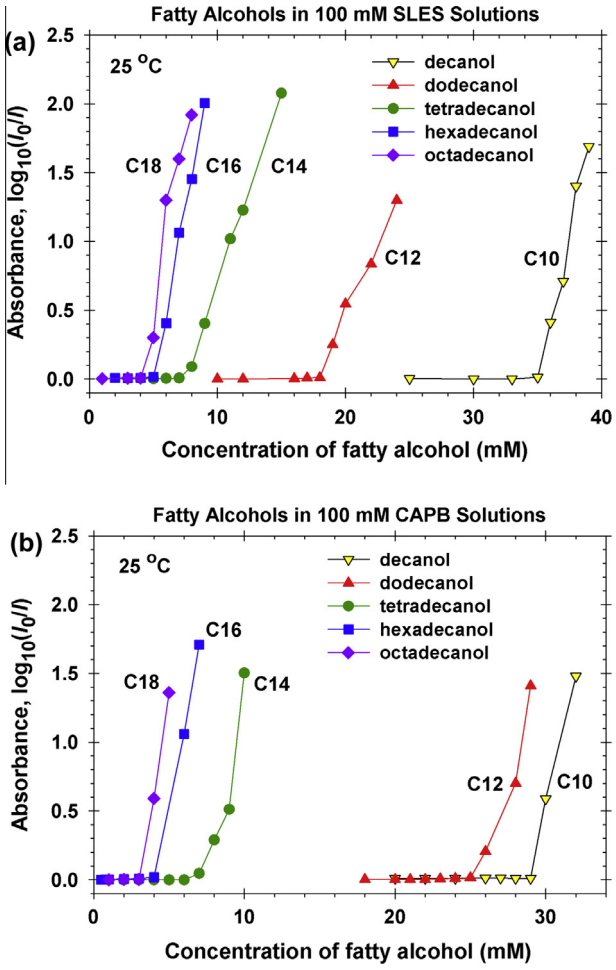

Fig. 1. Absorbance of light vs. the fatty alcohol concentration, C_A, for five alcohols at $T = 25$ °C. The surfactant solution is (a) 100 mM SLES and (b) 100 mM CAPB. The lines are guides to the eye.

where C_S is the total input concentration of surfactant (e.g. SLES) in the solution; $C_{A,sat}$ is the total input concentration of fatty alcohol in the solution at saturation (at the solubility limit). In Eq. (3.1), we neglect the amount of surfactant and fatty alcohol in *monomeric* form, because our measurements of $C_{A,sat}$ are carried out at concentrations much above the CMC, so that the predominant part of the amphiphilic molecules are present in micellar form.

3.2. Temperature dependence of the solubility limit

The temperature dependence of the solubility limit of fatty alcohols in micellar surfactant solutions is visualized in Fig. 2 in the form of plots of $y_{A,sat}$, vs. T for the investigated solutions. At all investigated temperatures, the general trend is $y_{A,sat}$ to decrease with the increase of the fatty-alcohol chainlength. More pronounced temperature dependence is observed for the alcohols with longer chains, whereas for $n = 10$ and 12 the dependence of $y_{A,sat}$ on temperature is rather weak. For $T \leqslant 35$ °C, a gap is present between the temperature dependences for the alcohols of shorter chains ($n = 10$ and 12) and longer chains ($n = 14$, 16 and 18). The temperature dependences of the solubility limit for SLES and CAPB are qualitatively similar; compare Fig. 2a and b.

3.3. Fatty-alcohol saturation concentration vs. surfactant concentration

Eq. (3.1) can be represented in the form:

$$C_{A,sat} = A_{sat} C_S, \quad \text{where} \quad A_{sat} \equiv \frac{y_{A,sat}}{1 - y_{A,sat}} \tag{3.2}$$

The thermodynamic theory and the experiments on solubilization of fatty acids ($n = 10$–18) in SLES and CAPB solutions in [18] showed that $A_{sat} = \text{const.}$, so that the solubility limit $C_{A,sat}$ is a linear function of the surfactant concentration, C_S; see Eq. (3.2). To check whether the same dependence holds also for fatty alcohols, we measured the dependence of $C_{A,sat}$ on C_S for the investigated 5 alcohols (C_nOH, $n = 10$, 12, 14, 16, 18) in micellar solutions of SLES. The results presented in Fig. 3a indicate that for fatty alcohols $C_{A,sat}$ also grows linearly with C_S, so that the slope A_{sat} is constant. The thermodynamic arguments in favor of the relation $A_{sat} = \text{const.}$ are considered in Section 4.2.

The fact that A_{sat} is independent of the surfactant concentration, C_S, means that the same is fulfilled also for the molar fraction of the alcohol at saturation, $y_{A,sat}$; see Eq. (3.2). In other words, the values of $y_{A,sat}$ in Table 1 can be used at any surfactant concentration (above the CMC), whereas the values of $C_{A,sat}$ in the same table correspond to 100 mM surfactant concentration, at which the experiments (Fig. 1) have been carried out.

In Fig. 3b, the obtained values of A_{sat} for fatty alcohols (calculated from the data in Table 1 and Fig. 3a) are compared with the values of A_{sat} for fatty acids obtained in [18]. It is seen that the acids have a considerably higher saturation ratio than the alcohols, for both SLES and CAPB solutions. In other words, at each given surfactant concentration, the saturation concentration is higher

Table 1
Experimental solubility limits for straight-chain fatty alcohols in 100 mM surfactant (SLES or CAPB) solutions: Data for $C_{A,sat}$ and $y_{A,sat}$ vs. n at different temperatures.

n	25 °C		30 °C		35 °C		40 °C	
	$C_{A,sat}$ (mM)	$y_{A,sat}$	$C_{A,sat}$ (mM)	$y_{A,sat}$	$C_{A,sat}$ (mM)	$y_{A,sat}$	$C_{A,sat}$ (mM)	$y_{A,sat}$
SLES								
10	35	0.2593	35.5	0.2620	35.5	0.2620	36	0.2647
12	18	0.1525	27	0.2126	28	0.2188	29	0.2248
14	7	0.0654	10	0.0909	15	0.1304	22	0.1803
16	5	0.0476	7	0.0654	10	0.0909	14	0.1228
18	3.7	0.0357	5	0.0476	7	0.0654	9.5	0.0868
CAPB								
10	29	0.2248	32	0.2424	32	0.2424	32	0.2424
12	25	0.2000	27	0.2126	28	0.2188	29	0.2248
14	6	0.0566	10	0.0909	17	0.1453	25	0.2000
16	4	0.0385	6	0.0566	10	0.0909	14	0.1228
18	3	0.0291	4	0.0385	6	0.0566	8	0.0741

n is the number of carbon atoms in the alcohol molecule.
$y_{A,sat}$ is the molar fraction of the alcohol in the mixed micelles at saturation.

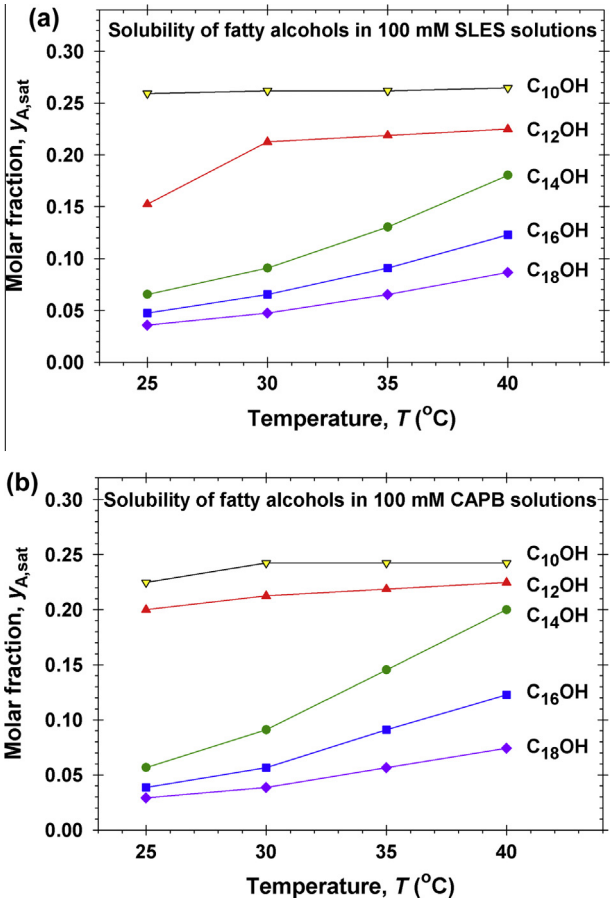

Fig. 2. Temperature dependence of the solubility of fatty alcohols in micellar surfactant solutions: Plot of the alcohol molar fraction at saturation, $y_{A,sat}$, vs. temperature, T, for five straight-chain saturated fatty alcohols. The surfactant solution is (a) 100 mM SLES, and (b) 100 mM CAPB. The lines are guides to the eye.

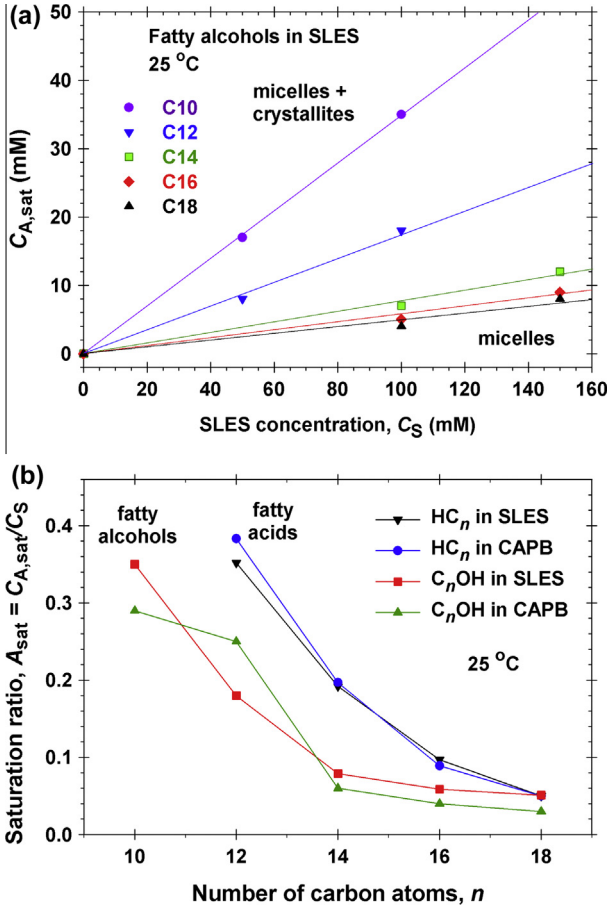

Fig. 3. (a) Plot of the fatty-alcohol (C_nOH) concentration at saturation, $C_{A,sat}$, vs. the surfactant (SLES) concentration, C_S for $n = 10$, 12, 14, 16 and 18. (b) Plot of the saturation ratio A_{sat} vs. the number of carbon atoms, n, in the molecules of the fatty acids and alcohols solubilized in SLES and CAPB. The lines are guides to the eye.

for the fatty acids. At the same n, the difference between fatty acids and alcohols is only due to their different headgroups. Consequently, the greater solubility of the fatty acids in SLES and CAPB micelles can be attributed to more favorable interaction of the headgroups of acid and surfactant in comparison with the headgroups of alcohol and surfactant.

At $n = 10$ and 12, the dependences of A_{sat} on n (Fig. 3b) are less regular, which is probably related to the fact that for these n values the mixture of alcohol and surfactant in the micelles behaves as a non-ideal solution (see below). For $n \geqslant 14$, the values of A_{sat} are close for SLES and CAPB.

4. Interpretation of the experimental data

4.1. Theoretical background

First, we briefly summarize the most important equations from solution thermodynamics. More details can be found in our previous paper [18]. The following notations will be used: x_i – mole fraction of component i dissolved in monomeric form; y_i – mole fraction of component i in the micelles (in the micellar pseudophase), and z_i – total mole fraction of component i contained in the solution. These molar fractions refer to the blend of amphiphilic molecules (the water is excluded). The surfactant mass balance reads [25]:

$$z_i C_T = (C_T - CMC_M) y_i + x_i CMC_M \tag{4.1}$$

C_T is the total concentration of all kinds of surfactant contained in the solution; CMC_M is the critical micellization concentration of the *mixed* surfactant solution. At equilibrium, setting equal the chemical potentials of the molecules of amphiphilic component i in monomeric and micellar form (Fig. 4), we obtain:

$$\mu^0_{i,mon} + kT \ln(x_i CMC_M) = \mu^0_{i,mic} + kT \ln(\gamma_i y_i) \tag{4.2}$$

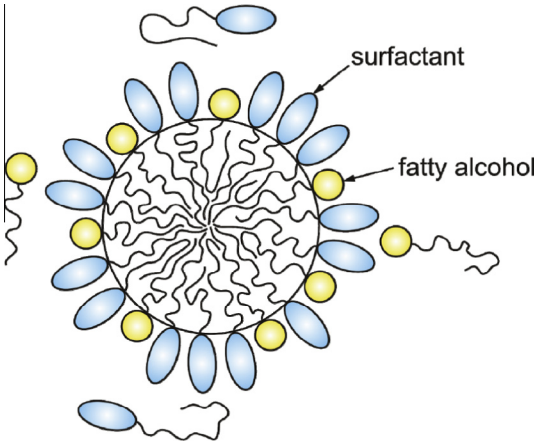

Fig. 4. Sketch of a mixed micelle composed of surfactant and fatty-alcohol molecules, which exist in equilibrium with free monomers in the surrounding aqueous phase.

$\mu^0_{i,\mathrm{mon}}$ and $\mu^0_{i,\mathrm{mic}}$ are the standard chemical potentials of the amphiphilic component i in monomeric form in water and in the micelles, respectively; γ_i is the activity coefficient of component i in the micelles; k is the Boltzmann constant and T is the absolute temperature. Eq. (4.2) is the form of the chemical-equilibrium relation for a nonionic amphiphile. The form of Eq. (4.2) for an ionic surfactant (like SLES) is considered in Section 6, where the effect of the electrostatic interactions is taken into account.

The micellization constant $K_{i,\mathrm{mic}}$ is related to the work for transferring of a monomer of component i from the solution into a micelle:

$$kT\ln K_{i,\mathrm{mic}} \equiv \mu^0_{i,\mathrm{mic}} - \mu^0_{i,\mathrm{mon}} \equiv \Delta\mu^0_{i,\mathrm{mic}} \tag{4.3}$$

Substituting Eq. (4.3) into Eq. (4.2) and taking inverse logarithm, we obtain:

$$\frac{c_i}{K_{i,\mathrm{mic}}} = \gamma_i y_i \tag{4.4}$$

where $c_i \equiv x_i \mathrm{CMC_M}$ is the concentration of monomers of the respective component. Eq. (4.4) is an equivalent of the Raoult's law stating that the concentration of component i in monomeric form is proportional to the activity, $\gamma_i y_i$, of this component in the micelles. (The conventional Raoult's law corresponds to $\gamma_i = 1$, i.e. to ideal mixing.) The form of Eq. (4.4) is analogous to the relationship between the molar fractions of the components in a liquid mixture, y_i, and the concentration of its vapors, c_i, as illustrated in Fig. 4.

For a given component, the working temperature can be *above* the Krafft temperature, T_{Krafft}, i.e. this surfactant forms micelles (rather than a precipitate of droplets or crystallites) [26,27]. For a solution containing only such surfactant, the equilibrium relation between micelles and monomers acquires the form $\mu^0_{i,\mathrm{mon}} + kT\ln \mathrm{CMC}_i \equiv \mu^0_{i,\mathrm{mic}}$, where CMC_i is the critical micellization concentration of the considered surfactant. The comparison of the latter equation with Eq. (4.3) leads to [25]:

$$K_{i,\mathrm{mic}} = \mathrm{CMC}_i \quad \text{for} \quad T > T_{\mathrm{Krafft}} \tag{4.5}$$

In our case, Eq. (4.5) will be applied to the zwitterionic CAPB, which effectively behaves as a nonionic surfactant (zero total charge of the molecule).

In the experimental temperature range, $25 \leqslant T \leqslant 40\ ^\circ\mathrm{C}$, the investigated fatty alcohols ($n = 10$–18) form precipitates in pure water, rather than micelles, i.e. for them $T < T_{\mathrm{Krafft}}$, so that Eq. (4.5) is inapplicable. For $i = \mathrm{A}$ (A = alcohol), Eqs. (4.2)–(4.4) refer to the exchange of alcohol monomers between the bulk and the mixed micelles with the basic surfactant (in our case SLES or CAPB). $K_{\mathrm{A,mic}} = K_{i,\mathrm{mic}}$ for $i = \mathrm{A}$ has the meaning of solubilization constant of the fatty alcohol in the micelles of the basic surfactant. In Section 4.4, $K_{\mathrm{A,mic}}$ is determined from the data for the solubility limit in Table 1.

4.2. Interpretation of the solubility limit

Following [18], we can explain the existence of solubility limit of the fatty alcohols in surfactant solutions on the basis of Eq. (4.4). The addition fatty alcohol (component A) to the solution leads to the increase of its mole fraction, y_A, in the micelles. From Eq. (4.4), it follows that the increase in y_A leads to an increase in the concentration c_A of fatty-alcohol monomers in the surrounding aqueous phase (Fig. 4). Precipitate of fatty alcohol (crystallites or droplets) appears when c_A reaches the solubility limit for the respective fatty alcohol in pure water, S_A. Then, Eq. (4.4) written for $i = \mathrm{A}$, acquires the form:

$$\frac{S_\mathrm{A}}{K_{\mathrm{A,mic}}} = \gamma_\mathrm{A}(y_{\mathrm{A,sat}})\, y_{\mathrm{A,sat}} \tag{4.6}$$

As before, $y_{\mathrm{A,sat}}$ is the value of y_A at saturation, and $\gamma_\mathrm{A} = \gamma_\mathrm{A}(y_{\mathrm{A,sat}})$ reflects the circumstance that the micellar activity coefficient, γ_i, depends on the micelle composition, y_i.

For example, the theory of the regular solutions gives the following explicit expression for the dependence $\gamma_\mathrm{A} = \gamma_\mathrm{A}(y_{\mathrm{A,sat}})$ for a binary mixture (A = alcohol, S = surfactant) [28]:

$$\gamma_i = \exp[\beta(1-y_i)^2], \quad i = \mathrm{A,S} \tag{4.7}$$

where β is the interaction parameter:

$$\beta \equiv -\frac{cw}{2kT}, \quad w = w_{\mathrm{AA}} + w_{\mathrm{SS}} - 2w_{\mathrm{AS}} \tag{4.8}$$

Here, c is the average number of closest neighbors of a given molecule in a micelle; w is the net interaction energy of a given molecule with its neighbors; w_{ij} is the energy of interaction between two closest neighbor molecules of type i and j. As a rule, w_{ij} is negative (attraction between two neighboring molecules) [28]. In contrast, w can be either negative, positive or zero. If $w = 0$, the micellar pseudophase represents an ideal mixture of its components (neutral mixing). The cases $\beta < 0$ and $\beta > 0$ correspond to negative and positive deviations from the Raoult's law [see Eqs. (4.4) and (4.8)], i.e. to energetically favorable and unfavorable mixing of the two components, respectively.

In view of Eq. (4.7), Eq. (4.6) represents an implicit equation for determining $y_{\mathrm{A,sat}}$. The left-hand side of Eq. (4.6) is a ratio of two constants, independent of the surfactant concentration, C_S. Consequently, $y_{\mathrm{A,sat}}$ must be also independent of C_S. Thus, we conclude that $A_{\mathrm{sat}} = y_{\mathrm{A,sat}}/(1 - y_{\mathrm{A,sat}})$ must be a constant, which is in full agreement with the experimental finding that the saturation concentration grows linearly with the surfactant concentration: $C_{\mathrm{A,sat}} = A_{\mathrm{sat}} C_\mathrm{S}$; see Fig. 3a and Eq. (3.2). This result supports the proposed explanation of the solubility limit on the basis of Eq. (4.6).

As mentioned in [18], Eq. (4.6) predicts that $C_{\mathrm{A,sat}}/C_\mathrm{S} = \mathrm{const.}$ irrespective of the specific form of the dependence $\gamma_\mathrm{A}(y_{\mathrm{A,sat}})$, i.e. of whether the regular solution model, Eq. (4.7), or another model is used. The relation $C_{\mathrm{A,sat}}/C_\mathrm{S} = \mathrm{const.}$ folds for both $\beta = 0$ and $\beta \neq 0$; see Eq. (4.7). Consequently, the linear dependences in Fig. 3a do not allow us to conclude whether the micelles represent an ideal or non-ideal mixture of surfactant and fatty alcohol.

4.3. Solubility limit of the fatty alcohols in pure water

Our next goal is to determine the fatty-alcohol solubilization constant $K_{\mathrm{A,mic}}$ and the interaction parameter β in Eq. (4.7) by means of a further analysis of the obtained experimental data. For this goal, we need the values of the fatty-alcohol solubility in pure water, S_A, for the five investigated alcohols ($n = 10$, 12, 14, 16 and 18) at the four working temperatures ($T = 25$, 30, 35 and 40 °C).

Data for the water solubility of normal straight-chain fatty alcohols were obtained by Maczynski et al. [29] and fitted with the equation:

$$\ln \hat{x}_1 = \ln \hat{x}_{1,\mathrm{min}} + C_1\left[\frac{T_{1,\mathrm{min}}}{T} - 1 - \ln\left(\frac{T_{1,\mathrm{min}}}{T}\right)\right] \tag{4.9}$$

Here, $\hat{x}_1$ is the solubility limit expressed as molar fraction; the temperature T should be expressed in °K; $\hat{x}_{1,\mathrm{min}}$, $T_{1,\mathrm{min}}$, and C_1 are constants determined in Ref. [29], which are summarized in Table 2.

From the molar fraction $\hat{x}_1$ calculated from Eq. (4.9) with parameter values from Table 2, one obtains the solubility of the respective alcohol, S_A:

$$S_\mathrm{A}[\mathrm{M}] = \frac{\hat{x}_1}{1-\hat{x}_1}\,\frac{1000 \times \rho_\mathrm{w}}{18.015} \tag{4.10}$$

where ρ_w [g/cm^3] is the density of water at a given temperature, and 18.015 g/mol is the molecular mass of water. The obtained

Table 2
The parameters $\ln \hat{x}_{1,\min}$, $T_{1,\min}$, and C_1 in Eq. (4.9): data from Ref. [29].

Alcohols	n	$\ln \hat{x}_{1,\min}$	$T_{1,\min}$ (K)	C_1
1-Decanol	10	−12.40	294.7	49.7
1-Undecanol	11	−13.77	290.9	53.9
1-Dodecanol	12	−15.13	287.7	58.1
1-Tetradecanol	14	−17.86	282.5	66.5
1-Hexadecanol	16	−20.60	278.4	74.9
1-Heptadecanol	17	−21.96	276.7	79.1

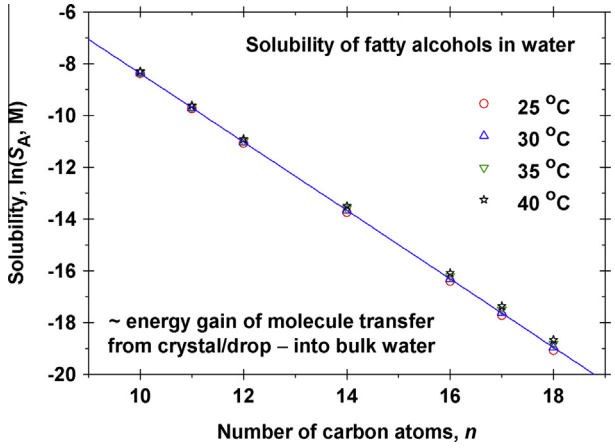

Fig. 5. Semi-logarithmic plot of the solubility of fatty alcohols in water, S_A, vs. the number of carbon atoms in the paraffin chain, n, at T = 25, 30, 35 and 40 °C. The line is the best fit of the data at 30 °C.

values of $\ln S_A$ at temperatures 25, 30, 35, and 40 °C, are shown in Fig. 5, where it is seen that the effect of T is relatively small and that $\ln S_A$ decreases linearly with the rise of the chainlength n. The illustrative straight line in Fig. 5 is the best fit of the data at T = 30 °C. For n = 18, the values of S_A at various T have been determined by extrapolation of the respective linear dependencies (Fig. 5); the results are given in Table 3.

The quantity $\ln S_A$ represents the energy gain from the transfer of a fatty-alcohol molecule from a fatty-alcohol droplet or crystal into the water phase, as a monomer:

$$kT \ln S_A \equiv \mu^0_{A,cryst} - \mu^0_{A,mon} \tag{4.11}$$

– compare Eqs. (4.11) and (4.3). As seen in Fig. 5, the magnitude of this energy difference linearly increases with the chainlength, n:

$$\ln S_A = a_0 + a_1 n \tag{4.12}$$

where a_0 and a_1 are parameters independent of n. Similar linear dependencies hold also for fatty acids, carboxylates, and acid soaps [18,30–32]. This fact is related to the energy for transfer of a CH_2 group from aqueous to non-aqueous environment, and is physically analogous to the known Traube's rule for the adsorption of surfactants from a given homologous series [33–35]. The values of a_0 and a_1, obtained from linear fits of the data in Table 3, are given in Table 4.

Table 3
The solubility limit, S_A (M), for saturated straight-chain fatty alcohols in pure water at various chainlengths n and temperatures.

n	S_A at 25 °C	S_A at 30 °C	S_A at 35 °C	S_A at 40 °C
10	2.29×10^{-4}	2.33×10^{-4}	2.40×10^{-4}	2.50×10^{-4}
12	1.55×10^{-5}	1.62×10^{-5}	1.70×10^{-5}	1.83×10^{-5}
14	1.07×10^{-6}	1.14×10^{-6}	1.24×10^{-6}	1.37×10^{-6}
16	7.46×10^{-8}	8.18×10^{-8}	9.12×10^{-8}	1.03×10^{-7}
18	5.19×10^{-9}	5.83×10^{-9}	6.69×10^{-9}	7.79×10^{-9}

Table 4
Values of a_0 and a_1 determined from the data in Table 3 for different temperatures.

T (°C)	$\ln S_A = a_0 + a_1 n$	
	a_0	a_1
25	4.95	−1.335
30	4.84	−1.322
35	4.74	−1.309
40	4.64	−1.295

4.4. Ideal vs. non-ideal mixing of surfactant and fatty alcohol in the micelles

In analogy with Eq. (4.12), for similar reasons the standard energy of transfer of a fatty alcohol molecule from an aqueous environment into the mixed micelle should be also a linear function of the chainlength, n:

$$\ln K_{A,mic} = k_0 + k_1 n \tag{4.13}$$

where k_0 and k_1 are parameters that are independent of n; see Eq. (4.3) and Refs. [18,25,36]. The values of k_0 and k_1 can be determined from the data for the solubility limits of fatty alcohols in surfactant micelles as explained below.

Taking logarithm of Eq. (4.6) and using Eqs. (4.7), (4.12) and (4.13), we obtain [18]:

$$\ln(y_{A,sat}) = q_0 + q_1 n - \beta(1 - y_{A,sat})^2 \tag{4.14}$$

where

$$q_0 = a_0 - k_0; \quad q_1 = a_1 - k_1 \tag{4.15}$$

From Eq. (4.14) it follows that for β = 0 (ideal solution), $\ln(y_{A,sat})$ should be a linear function of n. To check this theoretical prediction, the data for $y_{A,sat}$ vs. n from Table 1 are plotted in semi-logarithmic scale in Fig. 6.

For n = 14, 16 and 18, all 8 experimental curves in Fig. 6 comply with straight lines. In view of Eq. (4.14), we can hypothesize that the respective mixed micelles have ideal behavior (β = 0). The physical reason for this behavior can be the matching between the chainlengths of the respective alcohols and surfactants [37]. Note that both CAPB and SLES are blends of molecules of different hydrocarbon chains, which behave as a surfactant of effective chainlength C_{16} [18]. Alkyl chain mismatches normally require differences of at least 4 carbon atoms. Therefore, it is not surprising that the mixing with fatty acids of n = 14, 16 and 18 is ideal, whereas for n = 10 and 12 it is non-ideal. Setting β = 0 in Eq. (4.14), we obtain:

$$\ln(y_{A,sat}) = q_0 + q_1 n \quad (n = 14, 16, 18) \tag{4.16}$$

Table 5 shows the values of q_0 and q_1, which have been obtained by fitting the linear portions of the experimental curves in Fig. 6 with linear regressions in accordance with Eq. (4.16). From the data for a_0, a_1, q_0 and q_1 in Tables 4 and 5, the values of k_0, k_1, $K_{A,mic}$ and $\Delta\mu^0_{A,mic}/kT$ were calculated by using, consecutively, Eqs. (4.15), (4.13) and (4.3). The results are presented in Tables 5 and 6.

For n = 10 and 12, the experimental points are located above the aforementioned linear dependences (Fig. 6). In view of Eq. (4.14), this can be interpreted as indication for non-ideal mixing of the surfactant and fatty alcohol in the micelles, i.e. for $\beta \neq 0$. The physical reason for this behavior can be the mismatch between the chainlengths of the respective alcohols and surfactants, as

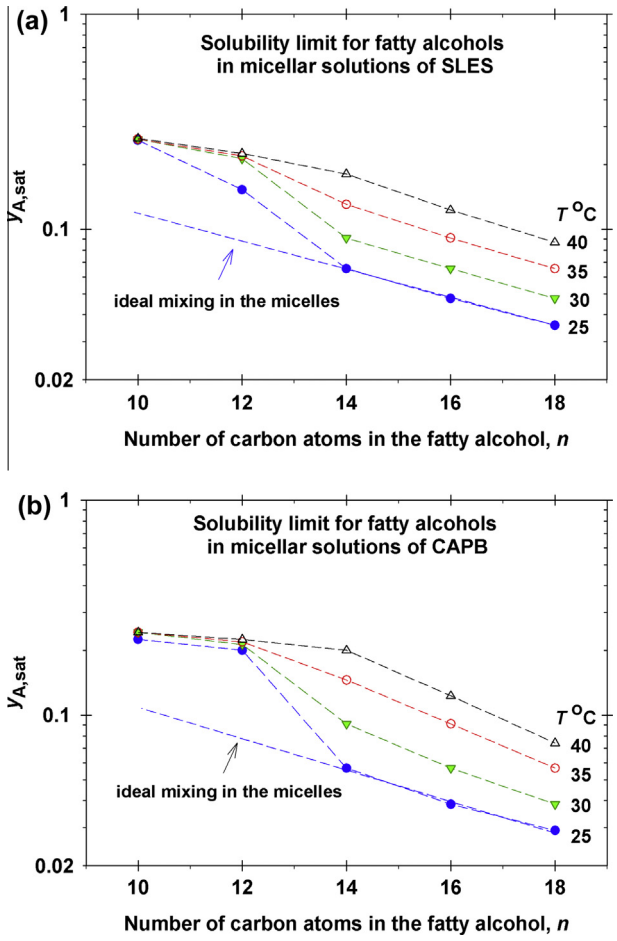

Fig. 6. The solubility limit, $y_{A,sat}$, vs. the number of carbon atoms in the paraffin chain, n, for five fatty alcohols (n = 10, 12, 14, 16, and 18) in (a) SLES and (b) CAPB solutions at four temperatures. For ideal mixing of surfactant and alcohol in the micelles ($\beta = 0$), the plots must be straight lines; see Eq. (4.14). Deviations from linearity indicate non-ideal mixing ($\beta \neq 0$). The lines are guides to the eye.

Table 5
Values of q_0 and q_1 determined from the data for n = 14, 16 and 18 in Fig. 6 by linear fits according to Eq. (4.16); k_0 and k_1 are calculated from Eq. (4.15) and Table 4.

T (°C)	C_nOH in SLES				C_nOH in CAPB			
	q_0	q_1	k_0	k_1	q_0	q_1	k_0	k_1
25	−0.613	−0.151	5.56	−1.19	−0.561	−0.166	5.51	−1.17
30	−0.136	−0.162	4.98	−1.16	0.595	−0.215	4.24	−1.11
35	0.373	−0.173	4.37	−1.14	1.372	−0.236	3.37	−1.07
40	0.839	−0.183	3.80	−1.12	1.870	−0.248	2.77	−1.05

mentioned above. The interaction parameter β can be determined from the expression [18]:

$$\beta = \frac{1}{(1 - y_{A,sat})^2} \ln\left(\frac{S_A}{y_{A,sat} K_{A,mic}}\right) \tag{4.17}$$

Eq. (4.17) follows from Eqs. (4.6) and (4.7). To calculate β, the respective values of $y_{A,sat}$, S_A and $K_{A,mic}$ from Tables 1, 3 and 6 have been substituted in Eq. (4.17). The obtained β values are given in Table 7, together with the respective values of the activity coefficient at saturation, $\gamma_{A,sat}$, calculated from Eq. (4.7) with $y_A = y_{A,sat}$.

4.5. Discussion

For n = 14, 16 and 18, the values in Table 7 indicate behavior close to ideal mixing, $\beta \approx 0$ and $\gamma_{A,sat} \approx 1$, as expected; see Fig. 6. For n = 10, 12 and T = 25, 30 °C we have $\beta < 0$, which indicates that the energy of the system decreases upon mixing of the fatty alcohol with the surfactant molecules in the micelles. This energy change favors the mixing, so that in the considered case the mixing is driven by both entropy and energy.

In contrast, for n = 10, 12 and T = 40 °C, we have $\beta > 0$, which means that at this higher temperature the energy of the system increases upon mixing, so that the spontaneous mixing is solely due to the raise of entropy. 35 °C is a transitional temperature: $\beta < 0$ for SLES, but $\beta > 0$ for CAPB (Table 7).

The values of the interaction parameter β in Table 7 are reasonable, having in mind that in all cases $\beta < 4$. In the regular solution theory [28], $\beta < 4$ means that the mixed micelles behave as a single pseudophase. In contrast, $\beta > 4$ would correspond to a phase separation, i.e. decomposition of the micellar pseudophase to two coexistent phases of different composition. Our experiments did not show any indications for such phase separation.

In Fig. 7, we compare the energy gains (in terms of standard chemical potentials) from the transfer of a fatty-alcohol molecule between two different phases at 25 °C for SLES. (In the case of CAPB, the respective graph is very similar to that for SLES.) As mentioned above, $kT \ln S_A = \mu^0_{A,cryst} - \mu^0_{A,mon}$ represents the energy gain at the transfer of a fatty-alcohol molecule from the fatty-alcohol crystallite or droplet into pure water, as a monomer. Curve A in Fig. 7 shows that this gain is negative, which means that the considered transfer is energetically disadvantageous and it happens only because of the rise in entropy of mixing. In addition, the decrease of $\ln S_A$ with n means that the considered transfer becomes more unfavorable with the rise of n. The magnitude of the slope $|a_1|$, which varies between 1.30 and 1.33kT, represents the transfer energy per CH_2 group; see Table 4 and Eq. (4.12). This energy is between the values given by the Traube's rule for the energy per CH_2 group during surfactant adsorption at air/water and oil/water interfaces, 1.1 and 1.6kT, respectively. (In the original Traube's rule for the air/water interface, the coefficient is $\ln 3 = 1.0986... \approx 1.1$.)

Curve B in Fig. 7 represents $-\ln K_{A,mic} = (\mu^0_{A,mic} - \mu^0_{A,mon})/kT$ vs. n, which is the energy gain at the transfer of a fatty-alcohol monomer from the water phase into a surfactant micelle. This gain is positive, which means that the considered transfer is energetically advantageous. In addition, the increase of $-\ln K_{A,mic}$ with n means that the considered transfer becomes more favorable with the rise of n. The magnitude of the slope $|k_1|$ that is close to 1.2kT (see Table 5), represents the respective transfer energy per CH_2 group, which is again close to the energy gain upon adsorption (the Traube's rule).

Curve C in Fig. 7 represents $(\mu^0_{A,cryst} - \mu^0_{A,mic})/kT$ vs. n, which is the energy gain at the transfer of a fatty-alcohol monomer from a fatty-alcohol crystal (or drop) into a surfactant micelle. (Curve C is the algebraic sum of curves A and B.) This gain is slightly negative, which means that the considered transfer is energetically disadvantageous and is driven solely by the entropy of mixing of components A and S in the micelles. The magnitude of the slope $|q_1|$ is in the range between 0.15 and 0.25kT [see Table 5 and Eq. (4.14)]; $|q_1|$ is considerably smaller than $|a_1|$ and $|k_1|$, and expresses the transfer energy per CH_2 group between two different *non-aqueous* phases: viz. a fatty-alcohol crystallite (or droplet) and the micellar pseudophase.

Fig. 8 shows plots of the solubilization energy per fatty-alcohol molecule, $-\Delta\mu^0_{A,mic} = -kT \ln K_{A,mic}$, vs. the fatty-alcohol chain-length, n, at different temperatures; see Table 6. The effect of temperature is relatively weak, and is better pronounced in the case of

Table 6
Solubilization constant, $K_{A,mic}$, and standard solubilization energy, $-\Delta\mu^0_{A,mic}/kT$, for fatty alcohols at various temperatures in SLES and CAPB micelles.

n	25 °C		30 °C		35 °C		40 °C	
	$\log K_{A,mic}$	$-\frac{\Delta\mu^0_{A,mic}}{kT}$	$\log K_{A,mic}$	$-\frac{\Delta\mu^0_{A,mic}}{kT}$	$\log K_{A,mic}$	$-\frac{\Delta\mu^0_{A,mic}}{kT}$	$\log K_{A,mic}$	$-\frac{\Delta\mu^0_{A,mic}}{kT}$
SLES								
10	−2.75	6.34	−2.88	6.62	−3.05	7.03	−3.21	7.40
12	−3.79	8.72	−3.88	8.94	−4.04	9.31	−4.17	9.64
14	−4.82	11.10	−4.89	11.26	−5.03	11.59	−5.16	11.88
16	−5.85	13.48	−5.90	13.58	−6.02	13.87	−6.13	14.12
18	−6.89	15.86	−6.91	15.90	−7.01	16.15	−7.11	16.36
CAPB								
10	−2.69	6.19	−2.98	6.86	−3.18	7.33	−3.36	7.73
12	−3.70	8.53	−3.94	9.08	−4.11	9.47	−4.27	9.83
14	−4.72	10.87	−4.91	11.30	−5.04	11.61	−5.18	11.93
16	−5.74	13.21	−5.87	13.52	−5.97	13.75	−6.09	14.03
18	−6.75	15.55	−6.84	15.74	−6.90	15.89	−7.00	16.13

Table 7
Values of the interaction parameter β and the activity coefficient $\gamma_{A,sat}$ determined from Eqs. (4.14) and (4.7) with q_0 and q_1 from Table 5 and $y_{A,sat}$ from Table 1.

n	HC_n in SLES		HC_n in CAPB	
	β	$\gamma_{A,sat}$	β	$\gamma_{A,sat}$
T = 25 °C				
10	−1.41	0.46	−1.21	0.48
12	−0.76	0.58	−1.47	0.39
14	0.00	1.00	−0.01	0.99
16	0.02	1.02	0.04	1.04
18	0.00	1.00	−0.01	0.99
T = 30 °C				
10	−0.76	0.66	−0.24	0.87
12	−0.86	0.59	−0.70	0.65
14	−0.01	0.99	−0.02	0.98
16	0.00	1.00	0.03	1.03
18	−0.01	0.99	−0.02	0.98
T = 35 °C				
10	−0.03	0.98	0.75	1.53
12	−0.30	0.83	0.10	1.06
14	−0.01	0.99	0.00	1.00
16	0.00	1.00	−0.01	0.99
18	−0.02	0.98	0.00	1.00
T = 40 °C				
10	0.63	1.40	1.41	2.24
12	0.23	1.15	0.64	1.47
14	−0.01	0.99	0.01	1.01
16	0.01	1.01	0.00	1.00
18	−0.01	0.99	0.01	1.01

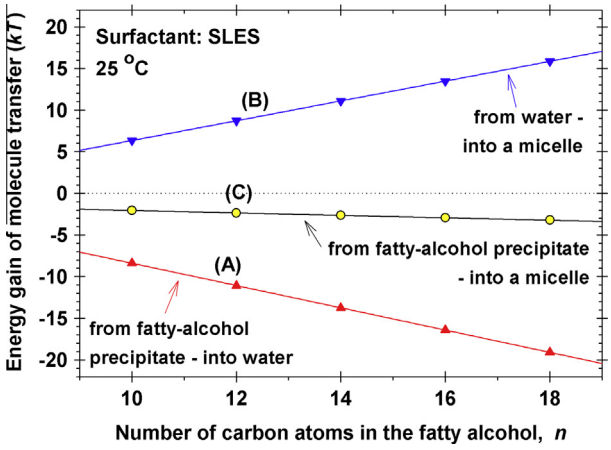

Fig. 7. Energy gain from the transfer of a fatty-alcohol molecule: Curve A – from fatty-alcohol precipitate (crystal or droplet) into water: $\mu^0_{A,cryst} - \mu^0_{A,mon} = kT \ln S_A$; curve B – from water into a surfactant micelle: $\mu^0_{A,mon} - \mu^0_{A,mic} = -kT \ln K_{A,mic}$, and curve C – from fatty-alcohol precipitate into a surfactant micelle: $\mu^0_{A,cryst} - \mu^0_{A,mic} = kT(\ln S_A - \ln K_{A,mic})$.

CAPB and at $n = 10$. The slope of the dependencies, $|k_1|$, which expresses the transfer energy per CH_2 group, decreases with the rise of T for both SLES and CAPB (see Table 5).

Fig. 9 compares the solubilization energies $-\Delta\mu^0_{A,mic} = -kT \ln K_{A,mic}$ for fatty alcohols (from Table 6) and fatty acids – from Table B.2 in [18]. It is seen that the energy gain upon solubilization is greater for both SLES (Fig. 9a) and CAPB (Fig. 9b) micelles. This result is in agreement with the experimental plot in Fig. 3b showing that at the same chainlength n, a given micellar solution can solubilize more fatty acid than fatty alcohol. As mentioned above, at the same n, the difference between fatty acids and alcohols is only due to their different headgroups. Hence, the greater solubility of the fatty acids in the investigated micellar surfactant solutions can be attributed to more favorable interaction of the headgroups of acid and surfactant in comparison with the headgroups of alcohol and surfactant.

It is interesting that for $n = 10$ and 12, at 25 and 30 °C $\beta < 0$ for fatty alcohols (Table 7), whereas $\beta > 0$ for fatty acids – see Table 6 in [18]. In other words, for these molecules of relatively shorter chains, *the mixing* is energetically favorable in the case of alcohols and unfavorable for acids. A possible explanation can be that the carboxylic group, –COOH, of the acids is more hydrophilic and inclined to H-bonding than the hydroxyl group, –OH, of the alcohols. The carboxylic group "anchors" the C10 and C12 fatty-acid molecule to the surface of the micelle, so that empty spaces (pockets) may appear within the micelles, which would be energetically unfavorable (Fig. 9c). Such an anchoring is missing for the C10 and C12 fatty-alcohol molecules. This additional degree of freedom leads to a minimization of the micelle free energy by a spontaneous adjustment of the location of the alcohol molecules within the micelle (Fig. 9c).

5. Phase diagrams for fatty alcohols in nonionic or zwitterionic surfactant solutions

This case is simpler because it is not necessary to take into account the effects of micelle surface electric potential and counterion binding, as in the case of ionic surfactants. To construct the diagram for fatty alcohols in CAPB solutions (Fig. 10a), here we will follow the procedure, which is described in details in Section 5 of Ref. [18]. It is convenient to create the diagram in terms of the total concentration of surface-active species, $C_T = C_A + C_S$, and the total input mole fraction of the fatty alcohol: $z_A = C_A/(C_A + C_S)$. As usual, C_A and C_S are the total input concentrations of fatty

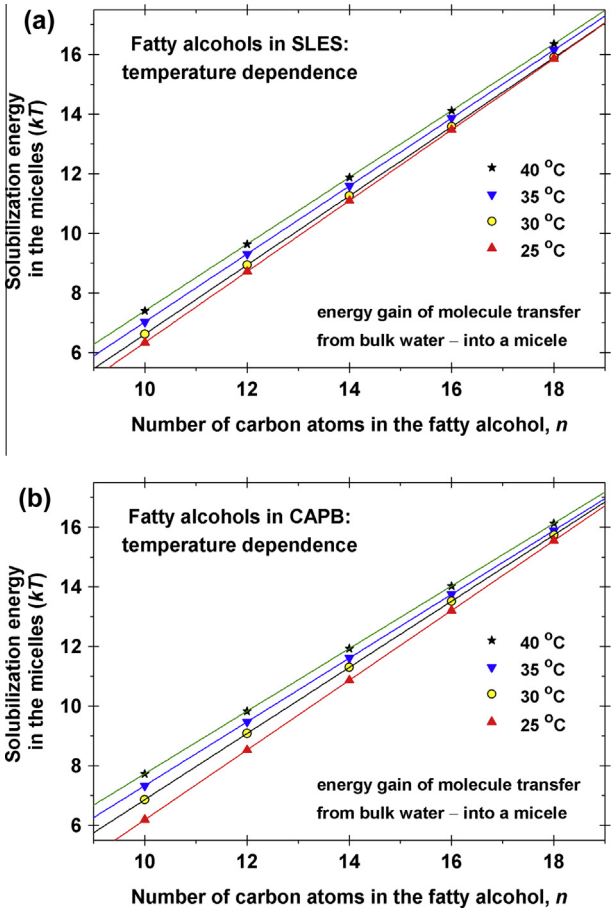

Fig. 8. Standard solubilization energy, $\Delta\mu^0_{A,mic}/(kT) = \ln K_{A,mic}$, vs. the number of carbon atoms in the fatty alcohol molecule, n, at different temperatures. (a) Fatty alcohols in SLES micelles. (b) Fatty alcohols in CAPB micelles.

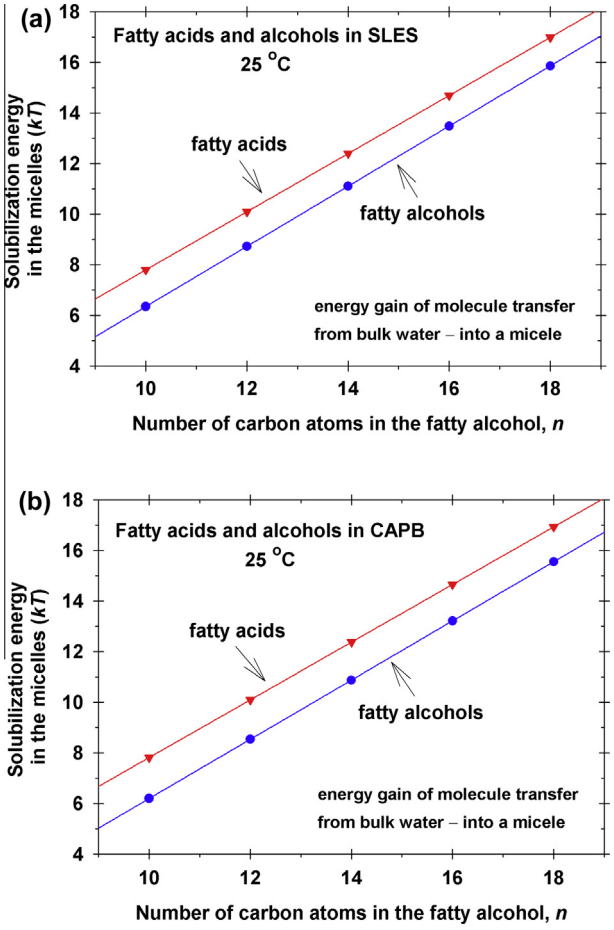

Fig. 9. Comparison of the solubilization energies, $-\Delta\mu^0_{A,mic}/(kT) = \ln K_{A,mic}$, of fatty acids and alcohols containing n carbon atoms vs. n at 25 °C in (a) SLES and (b) CAPB micelles. (c) Sketch of a micelle that contains fatty acid and fatty alcohol surrounded by the molecules of a surfactant with longer chain.

alcohol and surfactant in the solution. Both C_T and z_A are known from the experiment. A dilution of the solution with pure water corresponds to a decrease of C_T at fixed z_A, i.e. to a horizontal line in the phase diagram.

The phase diagram has four domains; see Fig. 10a. In the "micelles" domain, the solution contains mixed micelles of components A (fatty alcohol) and S (surfactant), but there is no fatty-alcohol precipitate (dispersed droplets or crystallites, depending on the temperature and chainlength). In the "micelles + precipitate" domain, the mixed micelles coexist with fatty-alcohol precipitate. In the domain denoted "precipitate", fatty-alcohol precipitate is present in the solution, but micelles are absent. Finally, in the "molecular solution" domain both micelles and precipitate are absent, and the solution contains only monomers of components A and S.

The basic parameters of the system are S_A, $y_{A,sat}$, $K_{A,mic}$ and $K_{S,mic}$. Values of S_A are given in Table 3, of $y_{A,sat}$ – in Table 1; of $K_{A,mic}$ – in Table 6; $K_{S,mic} = 9 \times 10^{-5}$ M is the CMC of CAPB. Further, β is determined from Eq. (4.17). The equations describing the inter-domain boundary lines (lines A, B, C, and D in Fig. 10a) can be found in Ref. [18]. All four boundary lines intersect in a quadruple point Q, whose coordinates (denoted by subscript Q) are:

$$C_{T,Q} = CMC_{M,sat}, \quad z_{A,Q} = \frac{S_A}{CMC_{M,sat}} \tag{5.1}$$

where $CMC_{M,sat}$ is the CMC of the mixed solution at $C_A = S_A$; see Ref. [18] for details. As seen in Fig. 10a, upon dilution of the mixed micellar solution (decrease of C_T at fixed z_A) we may have different behavior of the system depending on whether z_A is smaller or greater than $z_{A,Q}$. If $z_A < z_{A,Q}$, the micelles will disassemble to monomers when crossing the line D. If $z_A > z_{A,Q}$, the micelles will disappear when crossing the line B, but the fatty alcohol precipitate will remain; the latter disappears when crossing the line C upon a further dilution.

6. Phase diagrams for fatty alcohols in ionic surfactant solutions

6.1. The full system of equations

In our previous study [18], the ionic surfactant (SLES), was approximately treated as nonionic with an effective micellization

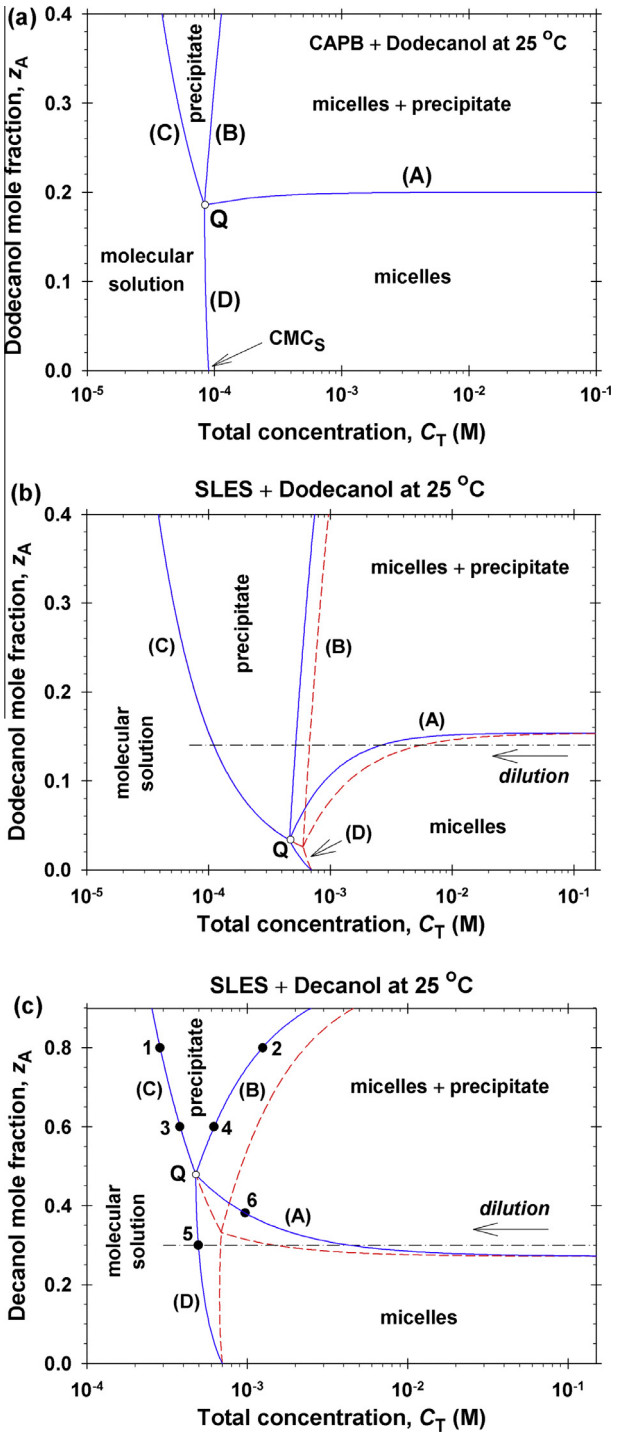

Fig. 10. Phase diagrams for solutions of surfactant and fatty alcohol. The lines A, B, C and D represent plots of the input mole fraction of alcohol, z_A, vs. the total concentration $C_T = C_S + C_A$ (surfactant + fatty alcohol) for the boundaries between the different phase domains. (a) Dodecanol in CAPB; (b) dodecanol in SLES, and (c) decanol in SLES; the solid and dashed curves are calculated by means of the detailed theory and the nonionic approximation, respectively; the experimental points correspond to the points/kinks with the same numbers in Fig. 12. Upon dilution (decrease of C_T at fixed z_A) the phase trajectory of the system may cross several phase domains – see the horizontal dot-dashed lines.

constant $\widehat{K}_{S,mic}$ equal to the CMC of the ionic surfactant. This simpler approach will be further termed the *nonionic approximation*. Here, we construct the phase diagrams on the basis of the detailed theory of micellar solutions of ionic surfactants and mixtures of ionic and nonionic surfactants developed in Ref. [20]. This theory takes into account the effects of micelle surface electric potential and counterion binding. Hereafter, it will be termed the *detailed theory*. Finally, we compare the predictions of the detailed theory with the experiment, as well as with the nonionic approximation.

The model proposed in Ref. [20] is based on a full system of equations that are expressing (i) chemical equilibria between micelles and monomers; (ii) mass balances with respect to each component, and (iii) the mechanical balance equation by Mitchell and Ninham [38], which states that the electrostatic repulsion between the headgroups of the ionic surfactant is counterbalanced by attractive forces between the surfactant molecules in the micelle. In view of subsequent applications for the construction of phase diagrams, here the equations of this system are first given and, next, their physical meaning is specified, as follows [20]:

$$\ln(c_A) = \ln K_{A,mic} + \ln(\gamma_A y_A) \tag{6.1}$$

$$\gamma_A = \exp[\beta(1-y_A)^2] \tag{6.2}$$

$$\gamma_S = \exp(\beta y_A^2) \tag{6.3}$$

$$y_A + y_S = 1 \tag{6.4}$$

$$\ln(c_{IS}\gamma_\pm) = \ln K_{S,mic} + \ln(\gamma_S y_{IS}) + \Phi_s \tag{6.5}$$

$$\ln(c_{MS}) = \ln K_{S,mic} + \ln(\gamma_S y_{MS}) \tag{6.6}$$

$$c_{MS} = K_{St} c_M c_{IS} \gamma_\pm^2 \tag{6.7}$$

$$y_S = y_{IS} + y_{MS} \tag{6.8}$$

$$I = (C_{salt} + c_{IS} + c_M)/2 \tag{6.9}$$

$$\log\gamma_\pm = -\frac{A\sqrt{I}}{1 + Bd_i\sqrt{I}} + bI \tag{6.10}$$

$$\gamma_S y_S \gamma_0 = 4kT\left(\frac{2I}{\pi L_B}\right)^{1/2}\left\{\sinh^2\left(\frac{\Phi_s}{4}\right) + \frac{2}{\kappa R}\ln\left[\cosh\left(\frac{\Phi_s}{4}\right)\right]\right\} \quad \text{(at CMC)} \tag{6.11a}$$

Here, c_A, c_{IS} and c_{MS} are bulk concentrations of fatty alcohol, ionized and non-ionized surfactant molecules (monomers); c_M is the concentration of free counterions (in our case Na^+); C_{salt} is the concentration of added inorganic salt (if any); y_A, y_{IS} and y_{MS} are the molar fractions of the respective components in the micelle; $\gamma_\pm$ is the activity coefficient for the ionic species in the bulk; γ_A and γ_S are the activity coefficients of the fatty alcohol and surfactant molecules in the micelle; $K_{S,mic}$ is the micellization constant of the ionic surfactant; $\Phi_s = e|\psi_s|/(kT)$ is the dimensionless surface electric potential, with e being the electronic charge and ψ_s – the dimensional surface potential; K_{St} is the Stern constant; I is the solution's ionic strength; d_i is the diameter of the ion; A, B and b are empirical parameters; in our calculations we used $A = 0.5115\ M^{-1/2}$, $Bd_i = 1.316\ M^{-1/2}$ and $b = 0.055\ M^{-1}$ [39]; R is the micelle radius at the level of the micelle surface charges; $\kappa = (8\pi L_B I)^{1/2}$ is the Debye screening parameter; $L_B = e^2/(4\pi\varepsilon_0\varepsilon kT)$ is the Bjerrum length; ε_0 is the dielectric permittivity of vacuum and ε is the dielectric constant of the solvent (water); $L_B = 0.72$ nm for water at 25 °C; γ_0 is a constant parameter (non-electrostatic component of the micelle surface tension) that characterizes a given ionic surfactant; for details, see Ref. [20].

Eq. (6.1) expresses the equilibrium between the micelles and the surrounding aqueous phase with respect to the exchange of fatty alcohol molecules. Eqs. (6.2) and (6.3) are expressions for the activity coefficients of the two components in the micelle originating from the regular solution theory [28]. Eq. (6.4) is a standard relation between the molar fractions of the two components in the micelle. Eqs. (6.5) and (6.6) express the equilibrium between the micelles and the surrounding aqueous phase with respect to the exchange of ionized and non-ionized surfactant molecules, respectively. Eq. (6.7) expresses the chemical equilibrium between ionized and non-ionized surfactant molecules in the bulk. Eq. (6.8)

is the definition of y_S. Eq. (6.9) is the expression for the solution's ionic strength, which can be used at concentrations both below and above the CMC [20]. Eq. (6.10) is a semi-empirical expression for the activity coefficient originating from the Debye–Hückel theory [39]; the log is decimal and I is expressed in mol/L.

Eq. (6.11a) is the Mitchell–Ninham equation [38] adapted for the case of mixed ionic–nonionic micelles [20]. The right-hand side expresses the electrostatic component of the surface pressure of the micelle, which is counterbalanced by the attraction between the molecules in the micelles – in the left-hand side of Eq. (6.11a). Because of this balance of repulsion and attraction, the equilibrium micelles are in tension free state, like the phospholipid bilayers [20,40]. Eq. (6.11a) holds at the CMC and it is used for calculating the boundary lines B and D of the phase diagram. In contrast, the boundary line A enters deeply into the micellar region, where the counterions dissociated from the micelles give an essential contribution to the Debye screening of the electric field. In such a case, a generalized form of Eq. (6.11a) has to be used [20]:

$$\gamma_S y_S \gamma_0 = 4kT\left(\frac{2I}{\pi L_B}\right)^{1/2}\left\{H\sinh^2\left(\frac{\Phi_s}{4}\right) - \frac{v\Phi_s}{4}\frac{\frac{\Phi_s}{4} - \tanh\left(\frac{\Phi_s}{4}\right)}{H\sinh\left(\frac{\Phi_s}{2}\right)} + \frac{2}{\kappa R}\ln\left[\cosh\left(\frac{\Phi_s}{4}\right)\right]\right\} \tag{6.11b}$$

The function $H(\Phi_s)$ and the parameter v are defined as follows:

$$H(\Phi_s) \equiv \left[1 + v\frac{\sinh(\Phi_s) - \Phi_s}{\cosh(\Phi_s) - 1}\right]^{1/2} \quad \text{and} \quad v \equiv \frac{y_{IS}c_{mic}}{2I} < 1 \tag{6.12}$$

where c_{mic} is the number of all amphiphilic molecules (SLES + fatty alcohol) incorporated in micelles per unit volume of the solution. At the CMC, we have $c_{mic} \to 0$; then $v \to 0$, $H \to 1$, and Eq. (6.11b) reduces to Eq. (6.11a).

The mass balance equations for surfactant, alcohol and counterions read as follows:

$$c_{IS} + c_{MS} + (y_{IS} + y_{MS})c_{mic} = (1 - z_A)C_T \tag{6.13}$$

$$c_A + y_A c_{mic} = z_A C_T \quad \text{for} \quad c_A \leqslant S_A \tag{6.14}$$

$$c_M + c_{MS} + y_{MS}c_{mic} = (1 - z_A)C_T + C_{salt} \tag{6.15}$$

The parameters that enter the above system of equations are known. The values of $K_{A,mic}$ and β for various fatty alcohols are given in Tables 6 and 7. The value of the Stern constant, which characterizes the binding of Na^+ ions to sulfate headgroups is $K_{St} = 0.6529\ M^{-1}$ [41]. In Appendix A, from the fit of data for the dependence of the CMC of SLES on the concentration of added NaCl it is found that of $K_{S,mic} = 1.20 \times 10^{-5}$ M and $\gamma_0 = 1.85$ mN/m. These parameter values, together with Eqs. (6.1)–(6.15), allow us to calculate the boundary lines of the phase diagram (Fig. 10b and c), as follows.

6.2. Line D: (molecular solution)/micelles boundary

Line D represents the dependence of the critical micellization concentration on the composition of the mixed solution of SLES and fatty alcohol in the absence of alcohol precipitate. There is no added salt, $C_{salt} = 0$, and the micelle concentration is vanishing, $c_{mic} = 0$. Along the line D, there is no precipitate, except in the end point Q, so that the concentration of alcohol varies in the range $0 \leqslant c_A \leqslant S_A$. The algorithm of calculations is the following.

First, for a given value of c_A we calculate y_A and γ_A by solving numerically the system of equations, Eqs. (6.1) and (6.2). Next, γ_S and y_S are calculated from Eqs. (6.3) and (6.4).

Second, the system of eight equations, Eqs. (6.5)–(6.11a), plus the electroneutrality condition $c_{IS} = c_M$, is solved numerically to determine the eight unknown quantities c_{IS}, c_{MS}, c_M, y_{IS}, y_{MS}, Φ_s, I and $\gamma_\pm$. Finally, from Eqs. (6.13) and (6.14) we determine z_A and C_T for each given value of c_A ($0 \leqslant c_A \leqslant S_A$).

6.3. Quadruple point Q

The parameters at the quadruple point, Q, are calculated applying the algorithm for the line D at $c_A = S_A$. The obtained parameters are denoted with the subscript "Q". In particular, from Eqs. (6.1)–(6.11a) we determine $y_{A,Q}$, $y_{S,Q}$, $\gamma_{A,Q}$, $\gamma_{S,Q}$, $c_{IS,Q}$, $c_{MS,Q}$, $c_{M,Q}$, $y_{IS,Q}$, $y_{MS,Q}$, $\Phi_{s,Q}$, I_Q and $\gamma_{\pm,Q}$, and further, from Eqs. (6.13) and (6.14) with $c_{mic} = 0$ we find $z_{A,Q}$ and $C_{T,Q}$. Note that $y_{A,Q}$ is identical with $y_{A,sat}$; see Table 1.

Table 8 shows the values of $C_{T,Q}$ and $z_{A,Q}$ obtained for SLES as explained above, as well as for CAPB obtained by using the theory for nonionic/zwitterionic surfactants [18]. One sees that the values of $C_{T,Q}$ (the CMC at the quadruple point) are systematically higher for SLES in comparison with CAPB, which is understandable because SLES is an ionic surfactant of higher CMC. In contrast, z_A (the alcohol molar fraction at the quadruple point) is systematically higher for CAPB, which reflects the higher solubility limit of the fatty alcohols in the CAPB micelles.

6.4. Line C: (molecular solution)/precipitate boundary

Here, as everywhere in this paper, the precipitate is from fatty alcohol, which can be in the form of dispersed crystallites or droplets depending on the temperature and chainlength. At the boundary line C, we have $c_A = S_A$ and $z_A = x_A$, so that the relation $c_A = x_A C_T$ yields the equation of line C in the form:

$$z_A = \frac{S_A}{C_T} \quad (z_{A,Q} \leqslant z_A \leqslant 1) \tag{6.16}$$

Along the line C, the surfactant concentration c_S varies from 0 at $z_A = 1$ to $(1 - z_{A,Q})C_{T,Q}$ at the quadruple point.

6.5. Line B: (micelles + precipitate)/precipitate boundary

At this boundary, we have $c_A = S_A$. Eqs. (6.1)–(6.11a) form a full system of equations, which is identical to the system that determines the parameters' values at the quadruple point Q. Thus, we find that the surfactant concentration is constant along the line B and equal to that in the quadruple point: $c_S \equiv c_{IS} + c_{MS} = (1 - z_{A,Q})C_{T,Q}$; see Eq. (6.13) with $c_{mic} = 0$. Then, the total concentration of fatty alcohol is $C_A \equiv z_A C_T = C_T - (1 - z_{A,Q})C_{T,Q}$, from where we find the equation of line B:

$$z_A = 1 - (1 - z_{A,Q})\frac{C_{T,Q}}{C_T} \quad (z_{A,Q} \leqslant z_A \leqslant 1) \tag{6.17}$$

Eq. (6.17) is applicable to both SLES and CAPB. The values of $C_{T,Q}$ and $z_{A,Q}$ are given in Table 8.

Table 8
Coordinates of the quadruple point Q for fatty alcohols with different number of carbon atoms, n, at $T = 25$ °C.

n	SLES		CAPB	
	$C_{T,Q}$ (M)	$z_{A,Q}$	$C_{T,Q}$ (M)	$z_{A,Q}$
10	4.78×10^{-4}	4.79×10^{-1}	2.95×10^{-4}	7.77×10^{-1}
12	4.62×10^{-4}	3.35×10^{-2}	8.34×10^{-5}	1.86×10^{-1}
14	5.88×10^{-4}	1.82×10^{-3}	8.60×10^{-5}	1.24×10^{-2}
16	6.14×10^{-4}	1.21×10^{-4}	8.66×10^{-5}	8.61×10^{-4}
18	6.34×10^{-4}	8.18×10^{-6}	8.74×10^{-5}	5.94×10^{-5}

6.6. Line A: (micelles + precipitate)/micelles boundary

At this boundary, we have $c_A = S_A$ and the micellar parameters y_A, y_S, γ_A, and γ_S are constant and equal to those in the quadruple point Q, viz. $y_{A,Q}$, $y_{S,Q}$, $\gamma_{A,Q}$, and $\gamma_{S,Q}$, which are determined from Eqs. (6.1)–(6.4). Next, for each given value of the total surfactant concentration $C_S \geqslant (1 - z_{A,Q})C_{T,Q}$ we determine the nine parameters c_{IS}, c_{MS}, c_M, y_{IS}, y_{MS}, Φ_s, I, $\gamma_\pm$ and c_{mic} by solving numerically the system of 9 equations, Eqs. (6.5)–(6.10), (6.11b), (6.13) and (6.15) the last two equations with $(1 - z_A)C_T = C_S$ and $C_{salt} = 0$. In particular, in this way we determine the concentration of surfactant in micellar form, c_{mic}, which enters the final formulas. The equation of line A can be presented in a parametric form, $C_T = C_T(C_S)$ and $z_A = z_A(C_S)$, as follows:

$$C_T = C_S + S_A + y_{A,Q}c_{mic} \tag{6.18}$$

$$z_A = \frac{C_T - C_S}{C_T} = \frac{S_A + y_{A,Q}c_{mic}}{C_T} \tag{6.19}$$

At sufficiently large C_T values, the predominant part of the amphiphilic molecules in the solution are present in micellar form, so that $C_T \approx c_{mic}$ and $y_{A,Q}c_{mic} \gg S_A$. In this limit, Eq. (6.19) predicts that z_A tends to a constant value, $z_A \approx y_{A,Q} = y_{A,sat}$.

6.7. Phase diagrams for mixed solutions of dodecanol and decanol with SLES

Fig. 10b and c shows the calculated phase diagrams for the mixed solutions of dodecanol and decanol with SLES at 25 °C. The solid lines are calculated using the detailed theory presented in this section. The dashed lines are drawn by using the simpler theory from Ref. [18], i.e. by a formal treatment of the anionic SLES as a nonionic surfactant (nonionic approximation). As seen in Fig. 10c, for the phase diagram of the mixed solutions of decanol + SLES the difference between the nonionic approximation and the detailed theory is considerable. In contrast, for the phase diagram of the mixed solutions of dodecanol + SLES (Fig. 10b) this difference is relatively small. The computed phase diagrams for normal alcohols of longer chain, $n = 14$, 16 and 18, showed that this difference further decreases and becomes practically negligible. The reasons for such behavior are discussed in Section 6.10.

A pronounced difference between the phase diagrams in Fig. 10b and c is that for dodecanol the quadruple point is situated below the line A, whereas for decanol Q is above the line A. In view of the comments after Eq. (6.19), this means that for dodecanol $y_{A,Q} > z_{A,Q}$ whereas for decanol $y_{A,Q} < z_{A,Q}$. In other words, in the close vicinity of the quadruple point Q, the micelles are enriched in dodecanol, but deprived of decanol relative to the bulk composition characterized by $z_{A,Q}$. This result is not surprising having in mind the longer hydrophobic chain of dodecanol.

From the viewpoint of the full system of equations, the value of $y_{A,Q}$ is determined by solving the subsystem of Eqs. (6.1) and (6.2) at $c_A = S_A$. These equations contain only constants related to the fatty alcohol (such as S_A and $K_{A,mic}$), but they do not contain the micelle surface potential Φ_s. For this reason, $y_{A,Q}$ is the same for the detailed theory and for the nonionic approximation. This circumstance explains the coincidence of the lines A predicted by the two models (the solid and dashed lines in Fig. 10b and c) at $C_T \to \infty$, where $z_A \to y_{A,Q}$.

6.8. Changes in the mixed micellar solutions upon dilution

Having solved the full system of equations in Section 6.1, one could predict the variations of various properties of the considered mixed solutions as functions of their composition. As an example, let us consider the changes that happen in the micellar solutions upon dilution with water, i.e. upon the decrease of total (surfactant + alcohol) concentration C_T at fixed alcohol molar fraction z_A. Such dilution corresponds to a horizontal line in the diagrams in Fig. 10.

In particular, lets us consider the horizontal lines at $z_A = 0.14$ in Fig. 10b and $z_A = 0.3$ in Fig. 10c ($T = 25$ °C). The former horizontal line intersects the boundary lines A, B and C, whereas the latter horizontal line intersects the boundary lines A and D. Our goal here is to investigate the changes in the solutions' properties upon dilution, including the changes upon crossing the boundary lines between different phase domains. Fig. 11a, c, and e shows the parameter variations upon dilution at *decanol* molar fraction $z_A = 0.3$, whereas Fig. 11b, d, and f shows analogous variations at *dodecanol* molar fraction $z_A = 0.14$.

As seen in Fig. 11a, at the higher C_T values, the system is in the "micelles + precipitate" phase domain where the equilibrium concentration of alcohol monomers is constant, $c_A = S_A$, and so does the molar fraction of decanol in the micelles, $y_A = y_{A,sat}$. At the boundary line A, the precipitate of fatty alcohol disappears, and both c_A and y_A decrease upon a further dilution, in the "micelle" zone of the phase diagram. In contrast, in the case of dodecanol (Fig. 11b) c_A and y_A are constant at the lower C_T, between the B and A lines, whereas at the higher C_T, in the "micelles" region c_A and y_A level off at their values corresponding to the limiting case, in which almost the whole amount of surfactant and alcohol is present in micellar form.

Further, let us compare the variations of the concentrations of surfactant ions, c_{IS}, counterions, c_M, and of amphiphilic molecules (surfactant + alcohol) in micellar form, c_{mic}, for the cases of decanol (Fig. 11c) and dodecanol (Fig. 11d). In the left-down corner of the respective plots, $c_{mic} \to 0$ at the line D (the CMC in the absence of alcohol precipitate) and line B (the CMC in the presence of alcohol precipitate). In Fig. 11c and d, c_{mic} and c_M increase, whereas c_{IS} decreases with the rise of C_T. This is a typical behavior for ionic surfactants. In particular, the decrease of c_{IS} is due to the increase of the solution's ionic strength, which leads to a decrease of the electrostatic repulsion between the free surfactant ions and micelles, as well as between the surfactant ions in the micelles. This favors the incorporation of more surfactant ions in the micelles and leads to a lowering of the concentration of free surfactant monomers; see e.g. Ref. [20].

Finally, in Fig. 11e and f we compare the variations of the molar fractions of ionized and non-ionized surfactant molecules in the micelles, y_{IS} and y_{MS}, and of the micelle surface potential, ψ_s. Everywhere in this article, the term "non-ionized surfactant molecule" is used to denote surfactant ion with bound counterion, so that y_{MS} characterizes the degree of counterion binding, or the occupancy of the Stern layer at the micelle surface. Both y_{MS} and $|\psi_s|$ are somewhat greater for dodecanol in comparison with decanol. This is related to the fact that in the case of dodecanol the molar fraction of the alcohol in the micelles, y_A, is about two times lower than that for decanol, viz. $y_A = 0.14$ for dodecanol vs. $y_A = 0.27$ for decanol at $C_T = 0.15$ M; see Fig. 11a and b. Correspondingly, the fraction of the ionic surfactant (SLES) in the micelles with dodecanol is greater, which enhances the electrostatic effects in the case of dodecanol. The discussion on the electrostatic effects continues in Section 6.10.

It is worthwhile nothing that except the kinks of c_A and y_A at the boundary line A in Fig. 11a and b, the other quantities plotted in Fig. 11 do not exhibit any pronounced kinks. This fact is important for the interpretation of the surface tension isotherms in the next subsection.

6.9. Comparison of the detailed theory with experimental data

As already mentioned, the dilution of a given solution of SLES and fatty alcohol (decrease of C_T at fixed z_A) corresponds to a

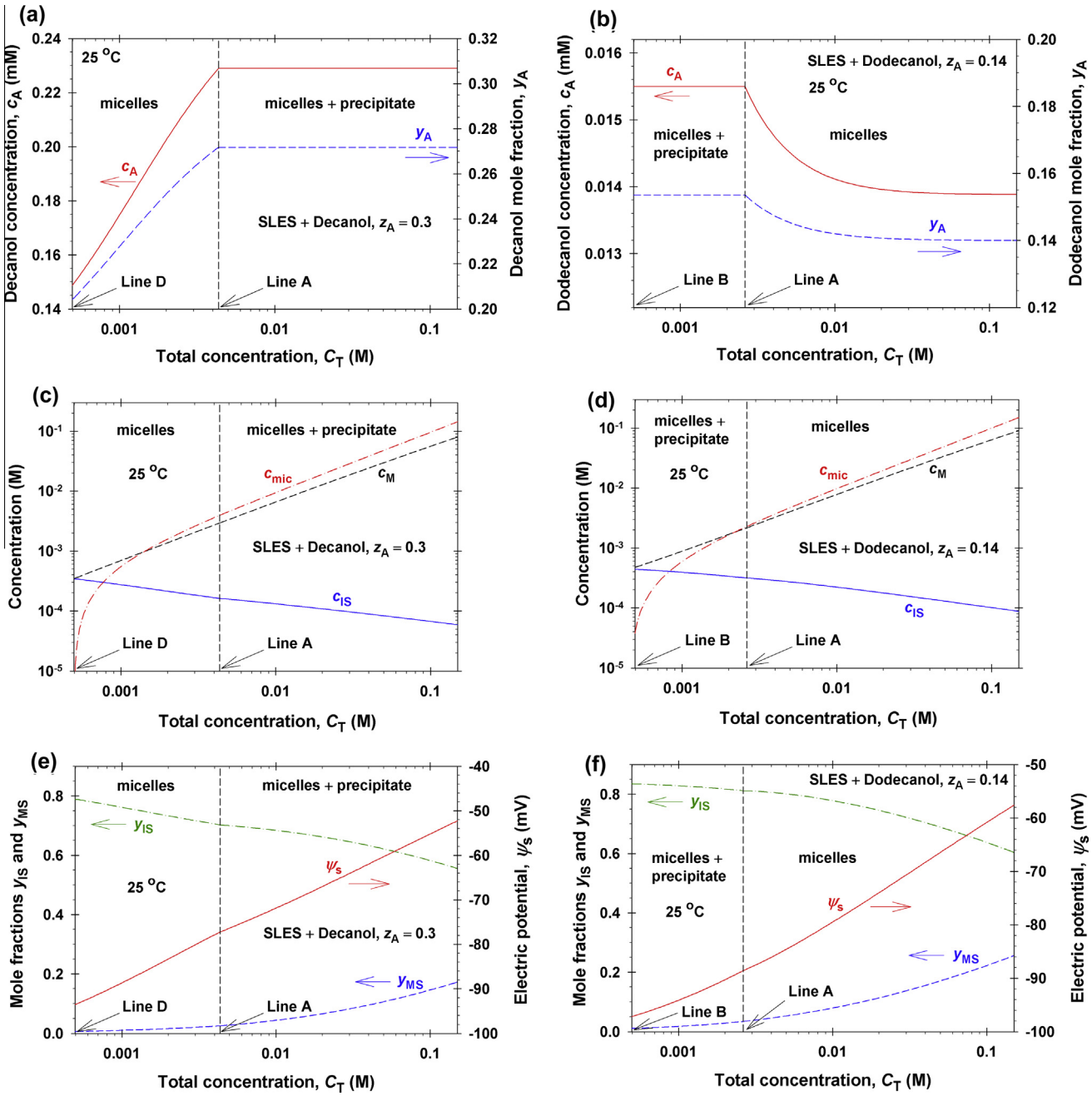

Fig. 11. Changes in the properties of mixed micellar solutions of (a, c, and e) SLES + decanol at $z_A = 0.3$, and (b, d, and f) SLES + dodecanol at $z_A = 0.14$ upon dilution, i.e. upon the decrease of C_T at fixed z_A; see the horizontal dash-dotted lines in Fig. 10b and c. (a and b) Plots of the concentration of free alcohol monomers, c_A, and alcohol molar fraction in the micelles, y_A. (c and d) Plots of the concentrations of free ionized surfactant monomers, c_{IS}; of counterions, c_M, and of amphiphilic molecules in micellar form, c_{mic}. (e and f) Plots of the molar fractions of ionized and non-ionized SLES molecules in the micelles, y_{IS} and y_{MS}, and of the micelle surface potential, ψ_s; in particular, y_{MS} characterizes the degree of counterion binding.

horizontal line in the phase diagram (Fig. 10). The intersection points of such a horizontal line with the boundary curves A, B, C and D should correspond to kinks in the experimental surface tension isotherms. To check this, we carried out surface tension measurements (by the du Noüy ring method with K100 apparatus, Krüss, Germany) for solutions with fixed $z_A = 0.3$, 0.6 and 0.8 M fraction of *decanol* at different stages of dilution. Decanol was chosen, because for its diagram (Fig. 10c) the difference between the detailed theory and the nonionic approximation is considerable.

The main plot in Fig. 12a is obtained at fixed $z_A = 0.8$; the kinks in points 1 and 2 correspond to the intersection of the phase trajectory of the system with the boundary lines C and B, respectively; see points 1 and 2 in Fig. 10c. The inset in Fig. 12a is obtained at fixed $z_A = 0.6$; the kinks in points 3 and 4 again correspond to the intersection of the phase trajectory with the boundary lines C and B, respectively; see points 3 and 4 in Fig. 10c. The kinks corresponding to intersection of line C are better pronounced than those corresponding to line B. Most probably, this is due to the fact that the surface concentration of the nonionic decanol is greater than that of the ionic SLES.

The main plot in Fig. 12b is obtained at fixed $z_A = 0.3$; the kink in point 5 corresponds to the intersection of the phase trajectory of the system with the boundary line D; see point 5 in Fig. 10c. The decrease of σ to the right of the point 5 in Fig. 12b is due to the rise

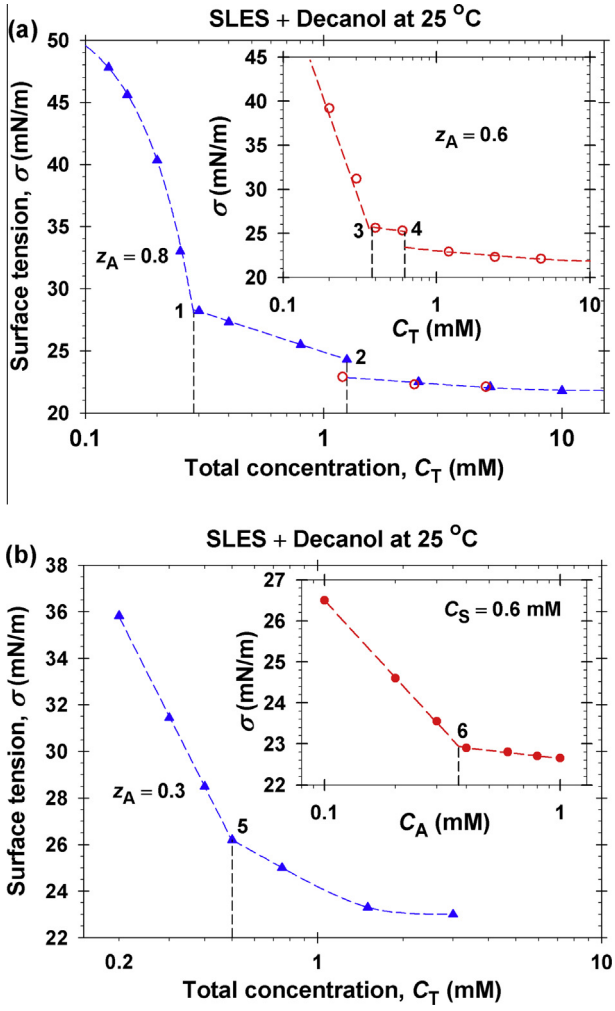

Fig. 12. (a) Plots of the surface tension σ vs. the total (surfactant + alcohol) concentration C_T at fixed $z_A = 0.8$ (the main plot) and $z_A = 0.6$ (the inset). (b) The main plot: σ vs. C_T at fixed $z_A = 0.3$. The inset: plot of σ vs. the input fatty alcohol concentration C_A at fixed SLES concentration, $C_S = 0.6$ mM. The points 1–6, which denote kinks in the experimental curves, correspond to intersections of the boundary lines in points denoted with the same numbers in Fig. 10c.

of c_A with C_T in the range $0.5 \leqslant C_T \leqslant 3$ mM; see Fig. 11a. The inset in Fig. 12b is obtained in a different way: The concentration of SLES is fixed, $C_S = 0.6$ mM, whereas the concentration of added decanol has been varied, $0.1 \leqslant C_A \leqslant 1$ mM. In this case, the kink in point 6 corresponds to the intersection of the phase trajectory of the system with the boundary line A; see point 6 in Fig. 10c. Both kinks in Fig. 12b are well pronounced.

The fact that the concentrations (C_T, z_A), corresponding to the kinks in the experimental surface tension isotherms in Fig. 12a and b, represent the coordinates of points, which are laying on the boundary lines of the calculated phase diagram in Fig. 10c, confirms the correctness of the detailed theory developed in the present section.

6.10. Effect of micelle electrostatic field on the phase diagrams

As already mentioned, the difference between the solid and dashed lines in Fig. 10b and c, calculated with the detailed theory and with the nonionic approximation are due to the effect of the micelle surface potential Φ_s, which is taken into account only in the detailed theory. Our goal here is to clarify why the difference between the phase diagrams predicted by the detailed and approximated theory is significant for decanol, but this difference becomes smaller for $n = 12$ (compare Fig. 10b and c) and negligibly small for $n \geqslant 14$. As seen in Fig. 10b and c, the electrostatic effect influences the position of the quadruple point Q, and the shapes of the lines A, B and D.

Let us focus our attention on the effect of Φ_s on the boundary line D, which represents the CMC of the mixed solutions as a function of composition (in the absence of alcohol precipitate), and which contains the quadruple point Q at its end. Taking inverse logarithms of Eqs. (6.1), (6.5) and (6.6), expressing y_A, y_{IS} and y_{MS} from the respective equations and substituting the results in the identity $y_A + y_{IS} + y_{MS} = 1$, we derive [20]:

$$\frac{1}{\mathrm{CMC_M}} = \frac{x_S}{\gamma_S K_{S,mic} e^{\Phi_s}} + \frac{x_A}{\gamma_A K_{A,mic}} \quad \text{(detailed model)} \tag{6.20}$$

Here, we have used the relation $c_i = x_i \mathrm{CMC_M}$ (i = A, S, MS), with $\mathrm{CMC_M}$ being the CMC of the mixed solution, as well as the approximations $c_S \approx c_{IS} \gg c_{MS}$ and $\gamma_\pm \approx 1$ that hold with a high accuracy at the low concentrations in the vicinity of the CMC. In the nonionic approximation, instead of Eq. (6.20), the following relation holds [18]:

$$\frac{1}{\mathrm{CMC_M}} = \frac{x_S}{\gamma_S \mathrm{CMC_S}} + \frac{x_A}{\gamma_A K_{A,mic}} \quad \text{(nonionic approximation)} \tag{6.21}$$

where $\mathrm{CMC_S}$ is the CMC of the ionic surfactant. Comparing Eqs. (6.20) and (6.21), we find that $K_{S,mic} e^{\Phi_s} \approx \mathrm{CMC_S} = \text{const.}$ in the nonionic approximation. The same approximation transforms Eq. (6.5) in the respective relation for a nonionic surfactant. In other words, the nonionic approximation does not neglect the effect of Φ_s, but assumes that Φ_s is constant. Hence, the differences between the solid and dashed boundary lines in Fig. 10b and c are due to variations in Φ_s, which are greater for decanol, but smaller for dodecanol and negligible for fatty alcohols of longer chain.

To verify the above statement, we calculated the micelle surface electric potential along the D line for the mixed solutions of SLES with fatty alcohols at $n = 10$–18. The results are presented in Fig. 13, where the alcohol mole fraction in the micelles, y_A, and the magnitude of the dimensional surface potential $|\psi_s|$ are plotted vs. the mole fraction of alcohol z_A, scaled with its value at the quadruple point, $z_{A,Q}$. All curves in Fig. 13a and b coincide in their left ends, which correspond to $z_A = 0$ and to the lower end of the line D in Fig. 10b and c. The differences between the curves in Fig. 13a and b are the greatest at $z_A/z_{A,Q} = 1$, i.e. at the quadruple point Q. In Fig. 13b, the upper horizontal line represents $|\psi_s|$ for SLES alone ($z_A = 0$). The variation of ψ_s is the greatest for decanol; smaller for dodecanol, and almost negligible for the fatty alcohols of longer chains. This result confirms the proposed explanation of the differences between the phase diagrams predicted by the detailed and approximated models (see the previous paragraph).

Physically, the decrease of the magnitude of the surface potential $|\psi_s|$ with the rise of z_A (Fig. 13b) is due to the increase of the molar fraction y_A of the nonionic component (the alcohol) in the micelles (Fig. 13a). This leads to a decrease in the surface charge density of the micelles and in their surface potential $|\psi_s|$. Among the investigated alcohols, this effect is the strongest for decanol (C10) and the weakest for octadecanol (C18). The physical reason for this is the strong decrease of the water solubility of the fatty alcohols with the rise of their chainlength (Fig. 5), which leads to a corresponding decrease in the concentration of alcohol monomers in equilibrium with the micelles (see the third column of Table 8) and, consequently, to a lower molar fraction of alcohol in the micelles (Fig. 13a).

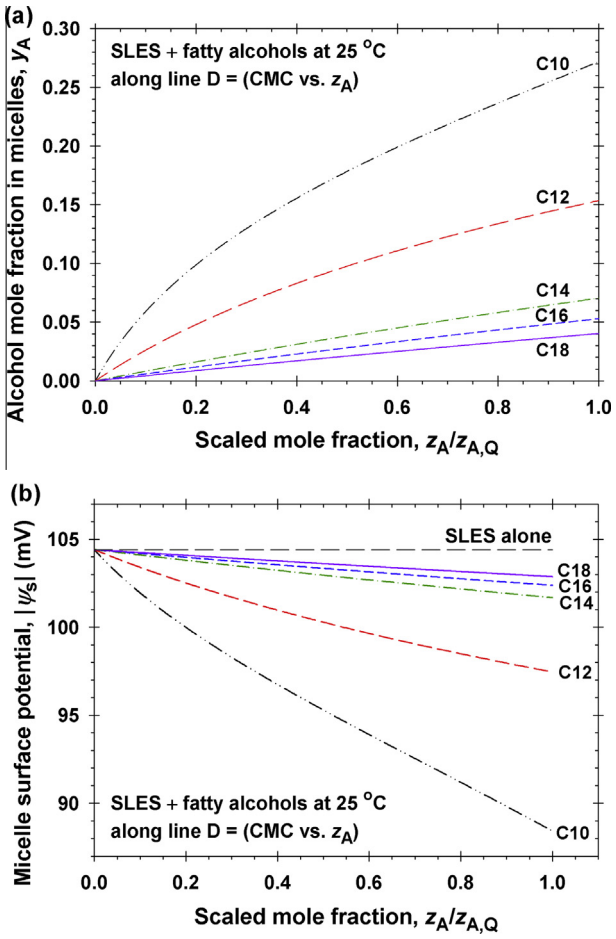

Fig. 13. Variations along the boundary line D of (a) the alcohol mole fraction in the micelles, y_A, and (b) the magnitude of the micelle surface electric potential, $|\psi_s|$, plotted vs. the alcohol mole fraction z_A, which is scaled with its value, $z_{A,Q}$, at the quadruple point, Q, for fatty alcohols with n = 10, 12, 14, 16 and 18 carbon atoms.

7. Conclusions

The solubility limits of fatty alcohols of medium (n = 10 and 12) and long (n = 14, 16, and 18) hydrocarbon chains in micellar solutions of the anionic surfactant SLES and the zwitterionic CAPB are experimentally determined by turbidity measurements at four temperatures: 25, 30, 35 and 40 °C. The solubility limits increase proportionally to the surfactant concentration, but strongly decrease with the rise of alcohol chainlength n (Fig. 3a). The temperature dependence of the alcohol molar fraction at saturation, $y_{A,sat}$, is not so pronounced (Fig. 2).

On the basis of the obtained experimental results, a quantitative theoretical interpretation of the solubility limit of fatty alcohols in surfactant micellar solutions is presented and a general picture of the phase behavior of the investigated systems is given in the form of phase diagrams. In particular, the limited solubility of fatty alcohols in the micelles of conventional surfactants is explained with the precipitation of their monomers in the bulk, rather than with micelle phase separation. The parameter of interaction between the components in the mixed micelles, β, is determined from the dependence of $y_{A,sat}$ on the alcohol chainlength n (Fig. 6). Having determined the solubilization constant $K_{A,mic}$ of a given alcohol from the data, we further calculate the boundary lines between the domains of the phase diagram of the mixed solutions (Fig. 10) by solving a system of chemical-equilibrium and mass-balance equations. In the case of ionic surfactant (like SLES), the system is formulated in terms of electrochemical potentials and complemented with the Mitchell–Ninham closure [38], which expresses the balance of repulsive (electrostatic) and attractive forces in the micelles (Section 6). The predicted positions of the boundary lines in the phase diagram agree very well with the kinks in experimental surface tension isotherms for mixed solutions of SLES and fatty alcohol (Fig. 12).

The long chain fatty alcohols (n = 14, 16 and 18) exhibit ideal mixing in the micelles of SLES and CAPB. Deviations from ideal mixing are observed for the fatty alcohols of shorter chain (n = 10 and 12), which can be explained by a mismatch with the longer chains of the surfactant molecules. In comparison with the fatty acids, the fatty alcohols exhibit a lower solubility in the micellar surfactant solutions (Fig. 3b) and lower solubilization energy (Fig. 9). This difference can be explained with a more favorable interaction of the headgroups of acid and surfactant in comparison with the headgroups of alcohol and surfactant. Moreover, at 25 °C and n = 10 and 12, the mixing of fatty alcohol and surfactant is energetically favorable ($\beta < 0$), whereas the mixing of fatty acid and surfactant is unfavorable ($\beta > 0$); see Table 6. A possible explanation is that alcohol molecules of relatively shorter chains can more freely adjust their position in the micelle to form a compact palisade layer, whereas the respective acid molecules are anchored by their hydrophilic headgroups to the micelle surface (Fig. 9c).

The approach for determining the solubilization constant $K_{A,mic}$ and the interaction parameter β for the mixed micelles, developed in Ref. [18] for fatty acids, is applied here to fatty alcohols. This approach is *alternative* to the Rubingh method [42] based on the dependence of CMC on the surfactant molar fractions in mixed solutions, which is difficult to apply for systems with low CMC, like those studied in the present paper. For both fatty acids and alcohols, the logarithms of $K_{A,mic}$ and of their limiting solubility in pure water S_A [29], depend linearly on the chainlength n (Figs. 5, 8 and 9), in analogy with the known Traube's rule [33–35]. The present results indicate that for n = 12 the nonionic approximation, used in Ref. [18] to calculate the phase diagram of lauric acid in SLES solution gives results, which are close to those of the detailed theory. The nonionic approximation gives accurate results for $n \geqslant 14$, but it fails for n = 10 (Fig. 10c). This can be explained with the decrease of the micelle surface potential, $|\psi_s|$, upon the addition of the nonionic alcohol. The effect is considerable for decanol, because (among the investigated alcohols) it exhibits the highest solubility in the micellar solutions and causes the greatest reduction in $|\psi_s|$ (Fig. 13), which can be quantified by using the detailed theory; see Section 6 and Ref. [20].

The results can find future applications for the understanding, quantitative interpretation and prediction of the phase behavior of various mixed micellar solutions of two (or more) amphiphilic compounds, one of them being water soluble and forming micelles, whereas the other one having a limited water solubility, but being soluble in the micelles of the former surfactant.

Acknowledgments

The authors gratefully acknowledge the support from Unilever R&D Trumbull, CT, USA; from the FP7 project Beyond-Everest, and from COST Action CM1101.

Appendix A. Supplementary material

"Determination of the micellar parameters for SLES from the dependence of CMC on the salt concentration", Supplementary data associated with this article can be found, in the online version, at http://dx.doi.org/10.1016/j.jcis.2014.09.042.

References

[1] K. Mysels, K. Shinoda, S. Frankel, Soap Films, Pergamon, London, 1959.
[2] D. Langevin, Adv. Colloid Interface Sci. 88 (2000) 209–222.
[3] D.A. Edwards, D.T. Wasan, J. Colloid Interface Sci. 139 (1990) 479–487.
[4] D.T. Wasan, in: K.L. Mittal, P. Kumar (Eds.), Emulsions, Foams, and Thin Films, Marcel Dekker, New York, 2000, pp. 1–30.
[5] W. Xu, A. Nikolov, D.T. Wasan, A. Gonsalves, R.P. Borwankar, Colloids Surf., A 214 (2003) 13–21.
[6] K. Tsujii, Surface Activity: Principles, Phenomena and Applications, Academic Press, London, 1998.
[7] B.D. Casson, C.D. Bain, J. Phys. Chem. B 103 (1999) 4678–4686.
[8] N.D. Denkov, S. Tcholakova, K. Golemanov, K.P. Ananthpadmanabhan, A. Lips, Soft Matter 5 (2009) 3389–3408.
[9] M. Durand, G. Martinoty, D. Langevin, Phys. Rev. E 60 (1999) R6307.
[10] A. Saint-Jalmes, D. Langevin, J. Phys.: Condens. Matter 14 (2002) 9397–9412.
[11] O. Pitois, C. Fritz, M. Vignes-Adler, J. Colloid Interface Sci. 282 (2005) 458–465.
[12] O. Pitois, C. Fritz, M. Vignes-Adler, Colloids Surf., A 261 (2005) 109–114.
[13] S. Tcholakova, Z. Mitrinova, K. Golemanov, N.D. Denkov, M. Vethamuthu, K.P. Ananthapadmanabhan, Langmuir 27 (2011) 14807–14819.
[14] N.D. Denkov, V. Subraminian, D. Gurovich, A. Lips, Colloids Surf., A 263 (2005) 129–145.
[15] K. Golemanov, N.D. Denkov, S. Tcholakova, M. Vethamuthu, A. Lips, Langmuir 24 (2008) 9956–9961.
[16] B. Dollet, J. Rheol. 54 (2010) 741–760.
[17] N.D. Denkov, S. Tcholakova, K. Golemanov, V. Subramanian, A. Lips, Colloids Surf., A 282 (2006) 329–347.
[18] S.S. Tzocheva, P.A. Kralchevsky, K.D. Danov, G.S. Georgieva, A.J. Post, K.P. Ananthapadmanabhan, J. Colloid Interface Sci. 369 (2012) 274–286.
[19] E. Mileva, J. Colloid Interface Sci. 232 (2000) 211–218.
[20] K.D. Danov, P.A. Kralchevsky, K.P. Ananthapadmanabhan, Adv. Colloid Interface Sci. 206 (2014) 17–45.
[21] M. Aoudia, T. Al-Maamari, F. Al-Salmi, Colloids Surf., A 335 (2009) 55–61.
[22] M. Aoudia, B. Al-Haddabi, Z. Al-Harthi, A. Al-Rubkhi, J. Surfactants Deterg. 13 (2010) 103–111.
[23] D. Vollhardt, G. Czichocki, R. Rudert, Colloids Surf., A 142 (1998) 315–322.
[24] D.R. Lide (Ed.), CRC Handbook of Chemistry and Physics, 86th ed., Taylor and Francis, Boca Raton, FL, 2006.
[25] M. Bourrel, R.S. Schechter, Microemulsions and Related Systems, M. Dekker, New York, 1988, p. 87.
[26] R.G. Laughlin, The Aqueous Phase Behavior of Surfactants, Academic Press, San Diego, 1994, p. 108.
[27] R. Klein, D. Touraud, W. Kunz, Green Chem. 10 (2008) 433–435.
[28] T.L. Hill, An Introduction to Statistical Thermodynamics, Dover, New York, 1987.
[29] A. Maczynski, D.G. Shaw, M. Goral, B. Wisniewska-Goclowska, J. Phys. Chem. Ref. Data 36 (2007) 685–731.
[30] J. Lucassen, J. Phys. Chem. 70 (1966) 1824–1830.
[31] P.A. Kralchevsky, K.D. Danov, S.D. Kralchevska, C.I. Pishmanova, N.C. Christov, K.P. Ananthapadmanabhan, A. Lips, Langmuir 23 (2007) 3538–3553.
[32] M.P. Boneva, K.D. Danov, P.A. Kralchevsky, S.D. Kralchevska, K.P. Ananthapadmanabhan, A. Lips, Colloids Surf., A 354 (2010) 172–187.
[33] A.W. Adamson, Physical Chemistry of Surfaces, fourth ed., Wiley, New York, 1982, p. 92.
[34] K.D. Danov, P.A. Kralchevsky, K.P. Ananthapadmanabhan, A. Lips, J. Colloid Interface Sci. 300 (2006) 809–813.
[35] J.N. Israelachvili, Intermolecular and Surface Forces, Academic Press, London, 2011.
[36] M.J. Rosen, Surfactants and Interfacial Phenomena, Wiley, New York, 1978, p. 88.
[37] P.C. Schulz, J.L. Rodriguez, R.M. Minardi, M.B. Sierra, M.A. Morini, J. Colloid Interface Sci. 303 (2006) 264–271.
[38] D.J. Mitchell, B.W. Ninham, J. Phys. Chem. 87 (1983) 2996–2998.
[39] R.A. Robinson, R.H. Stokes, Electrolyte Solutions, Butterworths, London, 1959.
[40] E.A. Evans, R. Skalak, CRC Crit. Rev. Bioeng. 3 (1979) 181–330.
[41] N.C. Christov, K.D. Danov, P.A. Kralchevsky, K.P. Ananthapadmanabhan, A. Lips, Langmuir 22 (2006) 7528–7542.
[42] D.N. Rubingh, in: K.L. Mittal (Ed.), Solution Chemistry of Surfactants, vol. 1, Plenum Press, New York, 1979, pp. 337–354.